University of Alberta

Chemiluminescence Detection in Microchip Capillary Electrophoresis and its Application to Immunoassays

by

Shakuntala Devi Mangru ©

A thesis submitted to the Faculty of Graduate Studies and Research in partial fulfillment of the requirements for the degree of Master of Science

Department of Chemistry

Edmonton, Alberta

Fall 1997

National Library of Canada
Acquisitions and Bibliographic Services
395 Wellington Street
Ottawa ON K1A 0N4
Canada

Bibliothèque nationale du Canada
Acquisitions et services bibliographiques
395, rue Wellington
Ottawa ON K1A 0N4
Canada

Your file Votre référence

Our file Notre référence

The author has granted a non-exclusive licence allowing the National Library of Canada to reproduce, loan, distribute or sell copies of this thesis in microform, paper or electronic formats.

L'auteur a accordé une licence non exclusive permettant à la Bibliothèque nationale du Canada de reproduire, prêter, distribuer ou vendre des copies de cette thèse sous la forme de microfiche/film, de reproduction sur papier ou sur format électronique.

The author retains ownership of the copyright in this thesis. Neither the thesis nor substantial extracts from it may be printed or otherwise reproduced without the author's permission.

L'auteur conserve la propriété du droit d'auteur qui protège cette thèse. Ni la thèse ni des extraits substantiels de celle-ci ne doivent être imprimés ou autrement reproduits sans son autorisation.

0-612-22633-6

Canada

University of Alberta

Library Release Form

Name of Author: Shakuntala Devi Mangru

Title of Thesis: Chemiluminescence Detection in Microchip Capillary Electrophoresis and its Application to Immunoassays

Degree: Master of Science

Year this Degree Granted: 1997

Permission is hereby granted to the University of Alberta Library to reproduce single copies of this thesis and to lend or sell such copies for private, scholarly, or scientific research purposes only.

The author reserves all other publication and other rights in association with the copyright in the thesis, and except as hereinbefore provided, neither the thesis nor any substantial portion thereof may be printed or otherwise reproduced in any material form whatsoever without the author's prior written permission.

Shakuntala D Mangru

Shakuntala Devi Mangru
805 Galbraith House
Michener Park
Edmonton, AB, T6H 5B5

1 st October, 1997

University of Alberta

Faculty of Graduate Studies and Research

The undersigned certify that they have read, and recommend to the Faculty of Graduate Studies and Research for acceptance, a thesis entitled Chemiluminescence Detection in Microchip Capillary Electrophoresis and its Application to Immunoassays submitted by Shakuntala Mangru in partial fulfillment of the requirements for the degree of Master of Science.

Dr. D. J. Harrison (Supervisor)

Dr. F. Cantwell

Dr. D. Li

Date 30 th Sept. 1997

To my husband, my parents and my brother

for their encouragement,

love and support.

ABSTRACT

Microchip capillary electrophoresis with laser induced fluorescence detection has become increasingly popular in recent years. This research was undertaken to demonstrate that chemiluminescence can be used for detection with these systems, utilizing post-column reactions on-chip. The horseradish peroxidase catalyzed reaction of luminol and hydrogen peroxide was chosen for this purpose. The chemiluminescent reaction was optimized for pH and both luminol and hydrogen peroxide concentrations, on-chip. A detection limit of 9 nM HRP-Fl was achieved by modifying the system. Among the modifications made were injecting a larger volume of sample, using a mirror at the detection region of the chip and using devices with larger capillary channels. The detection limit achieved was better than that obtained prior to any modifications by a factor of 1000. It was then demonstrated that the detection system can be applied to an analytically useful reaction. For this purpose, immunoassays were selected. The immunoreaction of $F(ab')_2$ fragment goat anti-mouse IgG, HRP conjugate directed against mouse IgG, whole molecule was studied. A calibration curve was constructed for the reaction and the affinity constant and average valency of the antibody was derived.

ACKNOWLEDGMENTS

I would like to thank Professor D. Jed Harrison, my supervisor for all he has done to make this project a reality. Without his support (both moral and financial), patience and guidance this research would not have been possible. I am grateful for the time he has sacrificed to correct my thesis. For all he has done, I'm truly thankful.

My gratitude goes out to Dr. Christa L. Colyer who has been a great friend and mentor. She took full responsibility for my training when I joined this research group. She has been extremely kind and patient with my persistent questions and has provided useful suggestions for guiding me along with my project. She gave me the encouragement and moral support I needed when things were not going well. I am very grateful for all she has done for me.

I am also extremely grateful to my husband who has made a great sacrifice to be here with me. He has provided me with all the moral support I can ever need and has been very kind, patient and understanding throughout my program. He has spent many late nights, doing anything in his power to help me along. His endless love and support knows no bounds. I cannot thank him enough for everything he has done.

I would like to thank my parents and my brother for the encouragement and support they provided me across the few thousand miles that separates us. I am grateful to my examiners Dr. F. Cantwell and Dr. D. Li for agreeing to read my thesis and to be on my committee on such a short notice. I would also like to express my sincere gratitude to my fellow group members for their support and the useful discussions they provided during my research. Special thanks to Laura MacDougall, Nghia Chiem, Gregor Ocvirk, Per Andersson, Thompson Tang and Loranelle Shultz-Lockyear for their help during the course of my research and thesis write-up. I am also thankful for financial support from the University of Alberta.

TABLE OF CONTENTS

CHAPTER 1

INTRODUCTION **1**

1.1 Capillary Electrophoresis 3

1.2 Microchip Capillary Electrophoresis 10

1.3 Chemiluminescence 11

1.3.1 Background *11*

1.3.2 Luminol Chemiluminescence *13*

1.4 Immunoassay 16

1.4.1 Classification of Immunoassays *17*

1.4.2 Antibodies *19*

1.4.3 Antibody-Antigen Interaction *21*

1.5 Summary 23

1.6 References 23

CHAPTER 2

OPTIMIZATION OF CHEMILUMINESCENT REACTION **27**

2.1 Introduction 27

2.2 Experimental 28

2.2.1 Device Fabrication *28*

2.2.2 Instrumentation *32*

2.2.3 Materials *34*

2.2.4 Procedures *35*

2.3 Results and Discussion 36

2.3.1 Preliminary Chemiluminescent Reactions *36*

2.3.2 On-Chip Experiments *38*

2.3.3 Sample Leakage 39
2.3.4 Luminol Optimization 41
2.3.5 Hydrogen Peroxide Concentration Study 45
2.3.6 Response to pH 47
2.4 CONCLUSIONS 50
2.5 References 51

CHAPTER 3

DETECTION LIMIT OF PEROXIDASE CONJUGATE 52

3.1 INTRODUCTION 52
3.2 EXPERIMENTAL 54
3.2.1 Device Fabrication 54
3.2.2 Instrumentation 55
3.2.3 Materials 55
3.2.4 Procedures 56
3.3 RESULTS AND DISCUSSION 57
3.3.1 Initial Detection Limit 57
3.3.2 Single-T Injection 57
3.3.3 Removal of Optical Filter 61
3.3.4 Mirror at the Detection Region 62
3.3.5 Response to PMT Voltage 64
3.3.6 Effect of a Higher N.A. Objective 67
3.3.7 Response to pH 67
3.3.8 Effect of Cooled PMT 69
3.3.9 Devices with Larger Channels 72
3.4 CONCLUSIONS 74
3.5 REFERENCES 78

CHAPTER 4

CHEMILUMINESCENT IMMUNOASSAYS IN MICROCHIP CAPILLARY ELECTROPHORESIS.....80

4.1 INTRODUCTION 80

4.2 EXPERIMENTAL.....82

4.2.1 Device Fabrication and Instrumentation *82*

4.2.2 Materials.....*83*

4.3 RESULTS AND DISCUSSION.....85

4.3.1 Preliminary Immunoassay Reaction.....*85*

4.3.2 Calibration Curve Without Internal Standard *87*

4.3.3 Calibration curve Using an Internal Standard.....*90*

4.3.4 Extended Calibration Curve.....*99*

4.4 CONCLUSIONS.....99

4.5 REFERENCES 102

CHAPTER 5

CONCLUSIONS 104

5.1 SUMMARY.....104

5.2 EVALUATION.....104

5.3 APPLICATIONS 105

5.4 FUTURE DIRECTIONS.....106

5.5 REFERENCES 107

LIST OF TABLES

TABLE 2-1 PYREX BONDING TEMPERATURE PROGRAM....31
TABLE 2-2 CHEMILUMINESCENT REACTIONS STUDIED....36
TABLE 4-1 SHOWING TREATMENT OF DATA OBTAINED WITHOUT INTERNAL STANDARD....91
TABLE 4-2 TREATMENT OF DATA OBTAINED WITH INTERNAL STANDARD....96
TABLE 4-3 TREATMENT OF DATA OBTAINED WITH INTERNAL STANDARD....97

LIST OF FIGURES

FIGURE 1-1 GENERAL SCHEMATIC OF A CONVENTIONAL CE INSTRUMENT 4

FIGURE 1-2 DIAGRAM ILLUSTRATING THE SEPARATION OF CHARGED AND UNCHARGED SPECIES IN CAPILLARY ELECTROPHORESIS 7

FIGURE 1-3 OUTLINE OF THE MECHANISM OF LUMINOL CHEMILUMINESCENCE 15

FIGURE 1-4 DIAGRAM ILLUSTRATING THE CLASSIFICATION OF IMMUNOASSAYS 18

FIGURE 1-5 BASIC STRUCTURE OF AN ANTIBODY MOLECULE 20

FIGURE 2-1 LAYOUT OF DEVICES PCRD 1 AND 2 29

FIGURE 2-2 DIAGRAM ILLUSTRATING THE MAIN FABRICATION STEPS FOR MICROCHIPS 30

FIGURE 2-3 DIAGRAM ILLUSTRATING THE INSTRUMENTAL SET-UP 33

FIGURE 2-4 ELECTROPHEROGRAM SHOWING LEAKAGE DURING SEPARATION 40

FIGURE 2-5 ELECTROPHEROGRAM SHOWING NO LEAKAGE 40

FIGURE 2-6 CHEMILUMINESCENCE RESPONSE TO LUMINOL CONCENTRATION USING HRP 42

FIGURE 2-7 CHEMILUMINESCENCE RESPONSE TO LUMINOL CONCENTRATION USING HRP-FL 44

FIGURE 2-8 CHEMILUMINESCENCE RESPONSE TO HYDROGEN PEROXIDE CONCENTRATION USING HRP-FL 46

FIGURE 2-9 CHEMILUMINESCENCE RESPONSE TO PH 48

FIGURE 2-10 NORMALIZED PEAK AREA FOR THE CHEMILUMINESCENCE RESPONSE TO PH 49

FIGURE 3-1 DIAGRAM ILLUSTRATING DOUBLE-T AND SINGLE-T INJECTIONS 59

FIGURE 3-2 ELECTROPHEROGRAMS COMPARING DOUBLE-T AND SINGLE-T INJECTIONS 60

FIGURE 3-3 ELECTROPHEROGRAMS SHOWING SIGNALS OBTAINED WITH AND WITHOUT FILTER 63

FIGURE 3-4 ELECTROPHEROGRAMS COMPARING SIGNALS OBTAINED WITH AND WITHOUT MIRROR AT THE DETECTION AREA 65
FIGURE 3-5 ELECTROPHEROGRAMS COMPARING SIGNALS OBTAINED AT DIFFERENT PMT VOLTAGES 66
FIGURE 3-6 ELECTROPHEROGRAMS COMPARING SIGNALS OBTAINED USING 0.35 N.A. AND 0.6 N.A. OBJECTIVES 68
FIGURE 3-7 ELECTROPHEROGRAMS OBTAINED AT DIFFERENT PH'S 70
FIGURE 3-8 COMPARISON OF SIGNALS OBTAINED WITH AND WITHOUT PMT COOLING 71
FIGURE 3-9 COMPARISON OF SIGNALS OBTAINED USING DEVICES WITH DIFFERENT SIZES OF CHANNELS 73
FIGURE 3-10 ILLUSTRATION OF DETECTION LIMITS ACHIEVED AFTER EACH MODIFICATION TO THE SYSTEM 75
FIGURE 4-1 ELECTROPHEROGRAMS SHOWING THE DECREASE IN AB* AS AG INCREASED 86
FIGURE 4-2 AB*-AG CALIBRATION CURVE WITHOUT INTERNAL STANDARD 88
FIGURE 4-3 ELECTROPHEROGRAM SHOWING ANTIBODY WITH MICROPEROXIDASE 93
FIGURE 4-4 AB*/MP RATIO VERSUS [AG] 95
FIGURE 4-5 AB*-AG CALIBRATION CURVE WITH INTERNAL STANDARD 98
FIGURE 4-6 EXTENDED AB*-AG CALIBRATION CURVE 100

CHAPTER 1

INTRODUCTION

Miniaturization of chemical analysis systems has attracted considerable interest over the past years, as a result of the advantages it offers compared to conventional systems. These include reduced sample and solvent consumption and decreased analysis times, leading to lower operation costs. In addition, it allows for a more compact, stable, portable system. It has been shown that capillary electrophoresis (CE) systems can be miniaturized by performing separations in capillary channels etched in a planar glass substrate.[1-7] This system allows for integration of complex networks of fluid channels which may be used for sample preparation, reagent delivery (for pH adjustment, derivatization, complexation etc.), and sample dilution steps, which are not as simple with conventional CE.[7] Solution manipulation is controlled by electroosmotic pumping, eliminating the need for pumps and valves. Using laser induced fluorescence for detection, the results achieved in the planar glass structures are comparable to that achieved in conventional CE.[5]

So far, laser induced fluorescence has been the most popular method of detection for microchip systems. Use of chemiluminescence should prove to be another step towards realizing a more compact, portable system. Since this method does not require a light source, it allows for a more simple optical detection system. Chemiluminescence has been used in conventional CE in several modes including on-column detection, post column detection and sheath flow cuvette. Research in combining CE with chemiluminescence detection has increased significantly in the recent years, although coupling the device with the chemiluminescence detector is

still problematic.[8] Most of the chemiluminescence detection done using conventional CE involves the tedious process of making T-connectors or inserting small diameter capillaries into larger diameter capillaries. The major difficulty in interfacing capillaries lies in the dead volume inherent in most junctions or connections between the capillary and the detector.[9] Band broadening can occur due to turbulence generated by the parabolic flow profile of reagents added by hydrostatic pressure at the junction. However, with a network of channels integrated on a glass chip and electroosmotic pumping of reagents, microchip capillary electrophoresis provides a simple alternative to coupling problems experienced by conventional CE. Staller and Sepaniak were able to construct post-capillary junctions via microscale molding for use as reactors.[9] However, this process was also tedious and was subject to some limitations which included use of different capillary sizes and limited choice of polymers for molding.

There have been several reports of chemiluminescent detection in immunoassays utilizing various chemiluminescent systems. Immunoassays are very specific reactions. This technique involves binding of an analyte (antigen) by an antibody molecule to produce an immune complex. Therefore, the amount of immune complex formed, or the amount of antibody consumed is a measure of the quantity of antigen present originally. Several methods can be used to determine the amount of immune complex formed, including radioactivity, fluorescence and chemiluminescence. This involves pre-labeling the antibody with either radioactive, fluorescent or chemiluminescent labels. For a number of years radioimmunoassays were widely used. However, due to the health hazards and waste disposal problems posed by these reagents, alternative methods are becoming more popular.

Use of microchip CE for immunoassays has been demonstrated using LIF detection.[10] Use of chemiluminescence detection of immunoreaction products

separated by microchip CE seems to be quite logical taking into consideration the advantages it offers. This research seeks to demonstrate that chemiluminescence detection can be applied to microchip based capillary electrophoresis for immunoassays.

1.1 Capillary Electrophoresis

Ever since Jorgenson and Lukas demonstrated the separation power and efficiency of capillary electrophoresis, it has stimulated a considerable amount of interest.[11, 12] Electrophoresis is a separation technique which takes advantage of the differential migration of sample ions relative to solvent under the influence of an external electric field. When this separation is performed in open tubular capillaries, the technique is referred to as capillary electrophoresis. There are several modes of capillary electrophoresis. These are capillary zone electrophoresis (CZE), capillary gel electrophoresis (CGE), capillary isoelectric focusing (CIEF), micellar electrokinetic chromatography (MEKC) and capillary isotachophoresis (CITP). The basic capillary electrophoresis instrument set-up is illustrated in Figure 1-1. Typically the capillaries used have 10-100 μm inner diameters and are 30-100 cm long. The capillaries used are most commonly made of fused silica.

In capillary zone electrophoresis, the capillary is filled with a buffer. The sample plug is introduced at the inlet and both ends of the capillary are immersed in buffer. A high voltage is applied to electrodes immersed in the inlet and outlet buffer reservoirs. In capillary electrophoresis, usually the inlet is positive and the outlet is negative. This is termed "normal" polarity. Separations performed with the inlet negative and the outlet positive is referred to as "reversed" polarity.

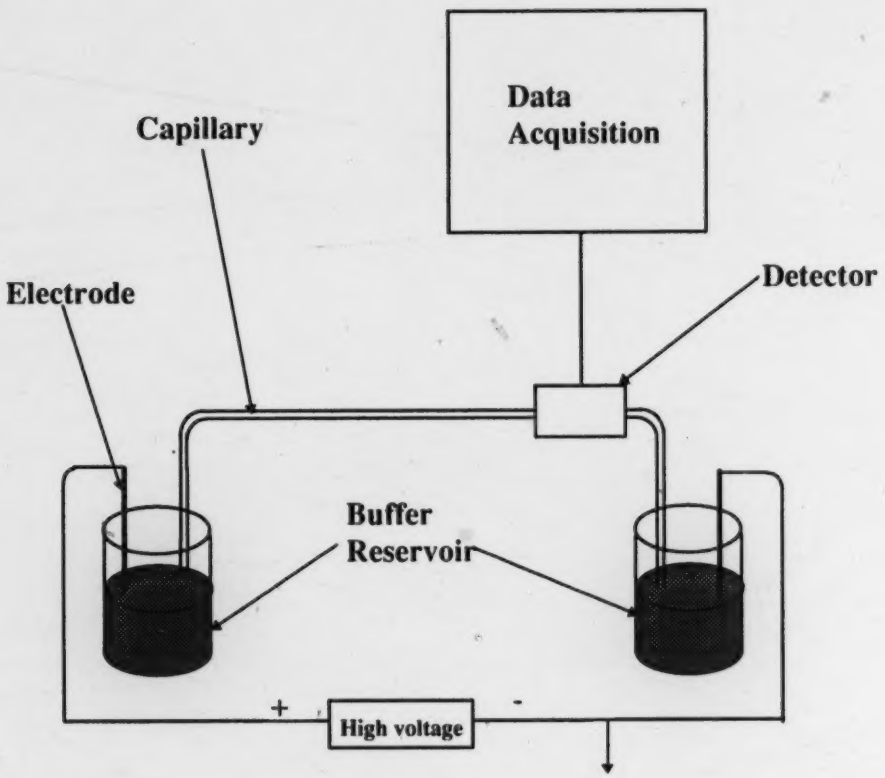

Figure 1-1 General Schematic of a Conventional CE instrument

Application of a voltage at the electrodes creates an electric field across the capillary. Electrophoresis is the result of migration of ionic species in a sample. The velocity and direction which these species migrate is dependent on their charge and size. Positive ions move towards the cathode and negative ions move towards the anode. Neutral species are not directly mobilized by the electric field. The migration is also affected by other factors such as frictional force and environment pH. Migration of an ion in an electric field due to its charge, size, frictional force and environment pH is called electrophoretic mobility.

Normally, capillary electrophoresis separations are performed at pH>3. In fused silica capillaries at pH>3, the capillary walls exhibit a negative charge due to the ionization of surface silanols.[13] Positive ions in the buffer solution align along the walls to form an electrical double layer creating a potential difference near the wall. This potential difference is known as zeta (ζ) potential. When an electric field is applied across the capillary, the positive ions will migrate towards the cathode carrying solvent molecules with them, resulting in bulk flow of solution. This flow, referred to as electroosmotic flow (EOF) is responsible for the transport of neutral species in the sample towards the outlet.

Electroosmosis transports solutes and solvents towards the cathode at the same speed and is not responsible for separation of sample components. Separation of sample species is generated by the differences in their electrophoretic mobilities. This separation is referred to as electrophoresis. Although electrophoresis moves anions to the anode and cations to the cathode, all species are transported to the cathode because electroosmotic mobility is usually higher than the electrophoretic mobility. Hence, the combined effects of electrophoretic mobility and electroosmotic flow are responsible for transport of all species towards the detector in CE. Therefore the net mobility of a species may be described by the following equation.

$$\mu_{net} = \mu_{eo} + \mu_{ep}$$

μ_{eo} is the electroosmotic mobility, μ_{ep} is the electrophoretic mobility and μ_{net} is the overall mobility. μ_{eo} and μ_{ep} can be further be defined as

$$\mu_{eo} = \varepsilon \zeta / 6 \pi \eta \quad \text{and} \quad \mu_{ep} = q / 6 \pi \eta \gamma$$

where ζ is the zeta potential, ε and η are the dielectric constant and viscosity of the solution and q and γ are the charge and hydrodynamic radius of the ion.[14]

The diagram in Figure 1-2 illustrates the concept of electrophoretic migration and electroosmotic flow.[15] Positively charged ions will elute first, followed by neutral and then negatively charged species. Positive species are transported by both electrophoretic and electroosmotic velocities. Neutral species migrate with the EOF and negative ions are transported towards the cathode by the EOF with an electrophoretic velocity acting in the opposite direction. The electropherogram sketched in Figure 1-2 shows the expected order of elution.

The zeta potential and hence EOF is dependent on both pH and ionic strength of the electrolyte.[15, 16] The pH of the buffer solution determines the fraction of silanol groups on the channel walls which are ionized. At high pH, the walls are negatively charged. Therefore, zeta potential is high and EOF is fast. At low pH EOF is slow and may even go in the opposite direction, since at pH<3 the walls will be positively charged. High ionic strength causes shielding of the surface charge on the channel walls thereby causing a drop in zeta potential and hence reduced EOF. Conversely, at low ionic strength, the EOF is increased.

There is one unique feature of electroosmotic flow in CE. Unlike pressure driven flow systems where the flow profile is parabolic, electroosmotic flow in CE has an almost flat flow profile across the width of the capillary. This results in very

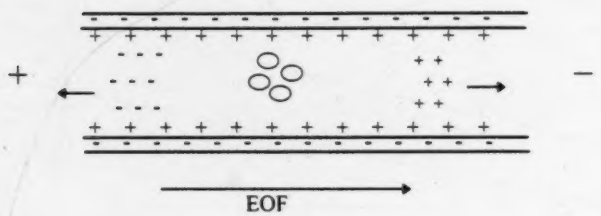

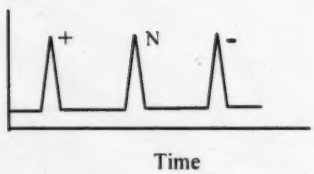

Figure 1-2 Diagram Illustrating the Separation of Charged and Uncharged Species in Capillary Electrophoresis

(Adapted from Ref. 15)

little bandbroadening, leading to very high separation efficiencies in CE. However, we cannot ignore the fact that longitudinal diffusion from electroosmosis can give rise to some broadening. Therefore, the time a sample spends on the capillary directly affects its separation efficiency and resolution. The migration time of an analyte is dependent on its electrophoretic mobility, as well as the electroosmotic flow. The velocity, v of the analyte is given by the following equation.

$$v = \mu_{net} E \quad \text{where} \quad E = V / L$$

E is the electric field, V is the applied voltage and L is the length of the capillary. Hence, migration time is given by

$$t = L^2 / \mu_{net} V$$

Therefore, migration time is also dependent on the length of the capillary and the voltage applied.

Another factor which should be considered in CE is Joule heating which results from the current in the capillary. Joule heating is undesirable because it can cause temperature and density gradients which can lead to bandbroadening. If severe enough, it can even result in boiling of solvent.[11, 17] However, due to the large surface area to volume ratio encountered in small bore capillaries used in CE, this is usually not a problem at powers less than 1W/m in fused silica capillaries or 2.5 W/m in glass chips.[6]

In capillary gel electrophoresis, instead of the capillary being filled with buffer, it is filled with a polymeric sieving gel. The capillary walls are usually coated in order to minimize electroosmotic flow which may cause extrusion of the gel. In addition, separation is usually done using reversed polarity.

Capillary isoelectric focusing involves the separation of mainly polypeptides in a pH gradient established across the capillary. The separation occurs due to differences in isoelectric points of the sample components. This method produces extremely narrow zones which improves resolution quite significantly, but is limited to molecules that have an isoelectric point (pI).

Micellar electrokinetic chromatography is used for the separation of neutral species, since they have no electrophoretic mobilities and hence cannot be separated by capillary zone electrophoresis. This is usually done by the addition of a charged species, to the separation buffer, which interacts with the neutral molecules to "induce" an electrophoretic velocity, thereby allowing separation of neutral molecules. The first additives used were micelles, hence the name micellar electrokinetic chromatography. This method may be extended to the separation of charged species which exhibit similar electrophoretic mobilities and hence cannot be separated by CZE.

Capillary isotachophoresis is employed for sample stacking purposes. With this method two separation buffers are used; one in front of the sample plug which is referred to as the leading electrolyte, and the other behind, called the terminating electrolyte. The buffers are prepared such that the leading electrolyte has a faster mobility than the sample and the terminating electrolyte has a slower mobility than the sample. Application of a high voltage causes the sample components (which is usually dissolved in the leading electrolyte) to align according to their mobilities between the two buffer regions. This results in sample plug concentration with the sample components focused into sharp bands. This is followed by normal capillary electrophoresis for separation of these zones.

1.2 Microchip Capillary Electrophoresis

A microchip capillary electrophoresis device consists of a manifold of interconnecting channels integrated on a planar substrate.[1, 5] Micromachining technology is used to fabricate these devices in glass.[6] Electroosmotic pumping is used for delivery of sample and reagents and electrophoresis is used for separation. The capillary channels are typically 1-10 cm in length and 30 μm wide with 10 μm depths. Due to the small dimensions of the device, very small sample and reagent volumes are required and separations are achieved in less than one minute.

Microchip systems are capable of handling several sample treatment steps on-chip.[7] These include sample preparation, reagent addition, dilution and quantitation. Since microchip CE consumes minute volumes of sample and reagents it is useful for samples which are not present in abundance, such as clinical samples. This technique also generates rapid results, making it suitable for on-site testing, as required by some environmental applications and clinical analyses.

Microchip CE with on-chip reactions automates sample preparation. In order to conduct complex reactions, several reagent addition steps are required. With conventional CE, reagent delivery is not as simple. It involves coupling of several capillaries using T-connectors, which automatically leads to problems with dead volume. In some cases, hydrostatic pressure is used to deliver reagents to the separation capillary, which may result in turbulence at the junction. Also, conventional CE systems tend to require larger sample and reagent volumes, and due to the length of the separation capillaries used, separations take longer than with microchip CE. Microchip CE systems provide a more simple means of delivering several reagents. Reagents are transported by electrokinetic effects thus eliminating

turbulent mixing at the junctions. In addition, junctions can be fabricated in microchips with almost zero dead volume.

Miniaturization and automation of a complete analysis typically involves sampling, sample treatment, separation, quantitation and data analysis on a small scale.[18] Any system which satisfies this criteria can be called a total analysis system (TAS) and when done on a small scale, may be called a micro-total analysis system (μ-TAS). Interest in μ-TAS is developing quite rapidly due to the advantages it offers. Due to automation, generation of results are fast, which can lead to greater throughput and even continuous monitoring for process control. Automation also reduces labor costs and can provide better reproducibility and accuracy since human errors are eliminated. Microchip CE is well suited for automation as it is capable of handling several sample preparation steps on-chip. Besides, only small volumes of sample and reagent are required. Except for the sampling step, microchip CE seems to satisfy the criteria for a total analysis system.

1.3 Chemiluminescence

1.3.1 Background

Chemiluminescence is the production of electromagnetic radiation from a chemical reaction in which an electronically excited species is generated, with subsequent relaxation to the ground state by the emission of a photon or by energy transfer to another molecule that then luminesces.[8, 19] Chemiluminescence is a dark field technique as it requires no excitation light and has several advantages for quantitative analytical applications. These include low detection limits, wide linear dynamic ranges, simple optical systems, fast response times and non-toxic reagent

systems. Since a source light is not required, there is no background from Rayleigh and Raman scattering resulting in this detection method being inherently sensitive as well as simple. This makes it an ideal candidate for detection on microchips, since the overall system peripherals would be more compact, stable and portable.

All light emission processes have similar characteristics in that they involve the production of an excited species followed by the return to ground state. However, it is the method of excitation and the return pathway to the ground state which determines the differences between these processes. For example, absorption of light energy may induce the transition of an electron from the singlet ground state (S_0) to a singlet excited state (S_1). Return of the electron from S_1 directly to S_0 results in emission, which is called fluorescence. However, if the electron transfers from S_1 to T_1, the triplet excited state, followed by return to S_0, the emission is called phosphorescence. In chemiluminescence, an excited molecule is generated from the chemical energy derived from a chemical reaction.[20-23] Therefore, most chemiluminescent reactions are high energy oxidation reactions. Return of the electron to the ground state is accompanied by emission producing chemiluminescence.

The efficiencies of chemiluminescent reactions are defined by the quantum yield, ϕ_{CL},[20, 24] which corresponds to the fraction of molecules emitting a photon upon return to ground state. The following equation defines the quantum yield.

$$\phi_{CL} = \phi_c \, \phi_e \, \phi_f$$

ϕ_c is the fraction of reacting molecules, ϕ_e is the fraction of molecules in an electronically excited state and ϕ_f is the fraction of molecules that emit a photon. Generally, the quantum yield is low, around 1 %.

Chemiluminescent intensity is a function of reactant concentration, which forms the basis for quantitation of chemical concentrations.[23] Chemiluminescence has a large linear dynamic range, which may be up to six orders of magnitude. According to Rongen et. al., the chemiluminescent response is usually "linearly proportional to the concentration, from the minimum detectable concentration up to the point where it is no longer possible to maintain an excess of reactant relative to the analyte."[20] Also, Nieman stated for luminol chemiluminescence, "within limits, chemiluminescence emission is directly proportional to the concentration of either luminol, or hydrogen peroxide, or catalyst..."[23]

The intensity of all chemiluminescent reactions vary with time. Typically, the signal increases upon initiation of reaction, passing through a maximum and then declining back to baseline. The chemiluminescence emission versus time profile varies from reagent to reagent. They can range from very rapid signal increases followed by either fast of slow decays or slow signal increases followed by fast or slow decays, or any other intermediate combinations. The total time of chemiluminescent emission may extend from a few minutes to several hours. Therefore, in flowing streams, it is extremely important to detect chemiluminescence emission at well defined periods in order to obtain maximum signal.

1.3.2 Luminol Chemiluminescence

Several chemiluminescent systems have been introduced since the first discovery of luminol chemiluminescence by Albrecht[25] in 1928. These included 1, 2-dioxetanes, acridinium esters, peroxyoxalates and luciferins. In addition, several derivatives of luminol have emerged, which are collectively termed acylhydrazides. Some of these systems require organic solvents to function, whereas with others,

aqueous solutions are sufficient. The horseradish peroxidase catalyzed reaction of luminol and hydrogen peroxide was chosen for our work, as the reaction was fairly simple and could be performed in aqueous solutions at a moderate pH.

Luminol is the common name for 5-amino-2,3-dihydrophthalazine-1,4-dione. However, it is also referred to as 3-aminophthalhydrazide and 3-aminophthalic acid hydrazide. The mechanism of luminol oxidation to produce chemiluminescence is well established and is outlined in Figure 1-3.[26] The first step involves the formation of a luminol radical which is oxidized to diazaquinone. This reacts with hydrogen peroxide eliminating nitrogen, with ring opening to produce phthalate in an electronically excited state. Relaxation of this molecule to the ground state results in chemiluminescence. Emission from luminol chemiluminescence is blue, centered at about 425 nm.

The oxidation of luminol by hydrogen peroxide is catalyzed by iron containing proteins called hematins. The emission is proportional to the amount of protein when excess substrate is present.[20] The most common protein catalysts are horseradish peroxidase, myleoperoxidase, microperoxidase and catalase. Other catalysts include Fe (III) complexes, ozone. Co (II) ions, halogens, persulphates and Cu (III) ions. Several reagents may be used to enhance the chemiluminescence in this system.[26-30] These include, p-iodophenol, 4-phenylboronic acids and some chemical indicators, just to name a few.

Chemiluminescence may be employed for detection in immunoassays as well as quantitative determination of other analytes. Since the luminol-hydrogen peroxide reaction is catalyzed by Fe (III) complexes, Co (II), Cu (II), Cr (III), Ni (II), Mn (II) and Ti (III) ions, it may be used for the detection of these species.[8, 19, 23] It can also

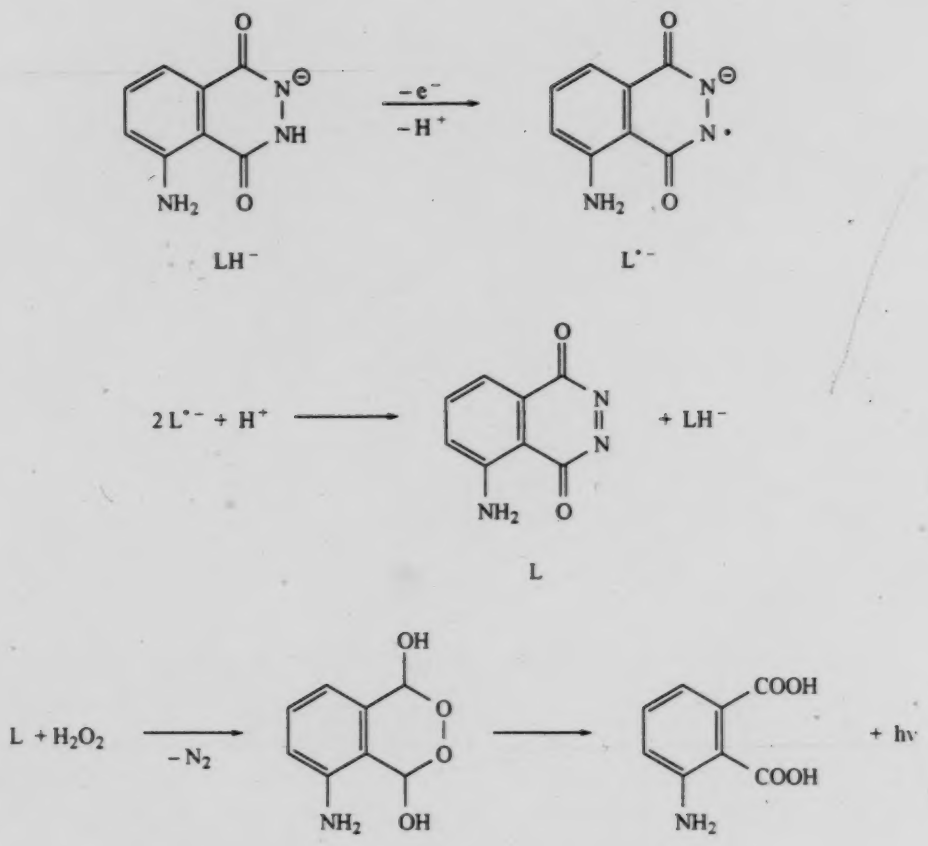

Figure 1-3 Outline of the Mechanism of Luminol Chemiluminescence (L represents Luminol)

be used for the detection of proteins and amino acids labeled with either HRP (or any of the other protein catalysts described above) or luminol (or any of its derivatives). The reaction may also be used for the detection of hydrogen peroxide either directly or by coupling to hydrogen peroxide producing reactions. Hydrogen peroxide is formed by the action of most oxidase enzymes. Hence analytes such as glucose, cholesterol, uric acid, sucrose and glucoside metabolites may be quantitated.[23] Therefore, this method can be quite useful for clinical, biochemical and environmental applications.

1.4 Immunoassay

Immunoassays are reactions which are capable of specifically detecting small quantities of a particular compound.[31] These assays are highly selective due to the natural ability of antibodies to bind to specific antigens. Immunoassays have become especially popular for the quantitation of biological and environmental analytes. Unfortunately, conventional immunoassay techniques tend to be slow, time consuming and labor intensive or involve large complex machinery for automation. Besides, they cannot easily provide the rapid, on-site results required by some clinical and environmental demands.

With the advent of CE, and more so microchip CE, there was hope for simpler automated systems. Application of CE to immunoassays has attracted considerable interest since its introduction in the early 90's. Kennedy et. al.,[32] Karger et. al.[33] and Chen et. al.[34, 35] were among the first to explore immunoassays coupled to CE. However, most of this work was done using traditional capillary electrophoresis. Harrison and Chiem successfully demonstrated the ability to conduct immunoassays using microchip CE with LIF detection.[10]

1.4.1 Classification of Immunoassays

There are several immunoassay formats. These are homogeneous and heterogeneous. From an immunology point of view, homogeneous assays do not require separation of the free and complexed fractions, whereas with heterogeneous assays, a separation step is required. However, from a chemistry perspective, an assay is termed homogeneous if it is done in a single phase and heterogeneous, if it requires several phases. Homogeneous and heterogeneous assays can be further classified as competitive and non-competitive. In competitive immunoassays a labeled and unlabeled antibody (or antigen) compete for a limited amount of antigen (or antibody). This assay is further classified as an immunoassay if the antigen is labeled or as an immunometric assay if antibody is labeled.[20] Non-competitive assays require an excess of reagents and are classified as direct or indirect. The assay is indirect when a secondary antibody is used against a second antibody, and direct when no secondary antibody is involved.[20] The diagram in Figure 1-4 summarizes the classes of immunoassays.

There are some other formats for classifying immunoassays based on the number of antibodies involved and the incubation times. For example, in a one site immunoassay the antigen is bound to one antibody and when the antigen is sandwiched between two different antibodies, it is called a two site assay.

In this research, we use a direct immunoassay which is classified as heterogeneous by immunologists since it involves a separation step, but homogeneous by chemists since it involves a single phase. By using an excess of labeled antibody to react with an unknown amount of antigen, the amount of antibody-antigen complex formed is a measure of the antigen present initially.

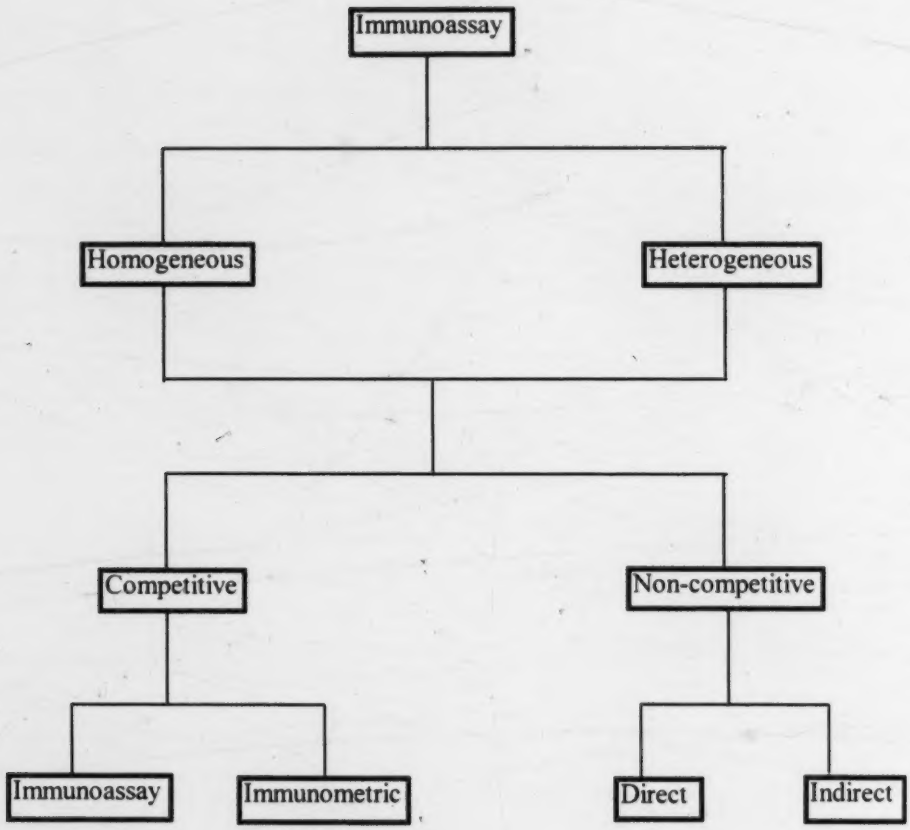

Figure 1-4 Diagram Illustrating the Classification of Immunoassays

1.4.2 Antibodies

Antibodies are proteins which are produced in the body in response to the presence of foreign molecules.[36] They circulate in the blood and lymph in the body, binding with foreign antigens. Removal of the antibody-antigen complexes from circulation occur through phagocytosis and serve to rid the body of pathogens and toxic substances.

Antibodies can be thought of as Y shaped molecules containing four polypeptides. Two of the polypeptides are identical and form the heavy chain of the molecule, while the other two are also identical and form the light chain. The type of heavy chain polypeptide and the number of Y-like units are used to classify antibodies as IgG, IgM, IgA, IgE and IgD. The diagram in Figure 1-5 illustrate the basic structure of an antibody molecule.

There are five different types of heavy chains and two different types of light chains. The heavy chains are Υ-chains found in IgGs, μ-chains found in IgMs, α-chains present in IgAs, ε-chains in IgEs and δ-chains contained in IgDs. The light chains are called κ and λ chains. A single antibody molecule will contain only one type of light chain and one type of heavy chain.

IgG molecules belong to the most simple class of antibodies. They contain only one structural Y unit and consist of three protein domains. The protein domains are comprised of two identical Fab domains and one F_c domain as illustrated in Figure 1-5. The heavy and light chains in the Fab domain and the two heavy chains in the F_c domain are cross-linked by di-sulphide bonds. Each Fab domain contain an antigen binding site. The F_c domain is responsible for immune response. The two

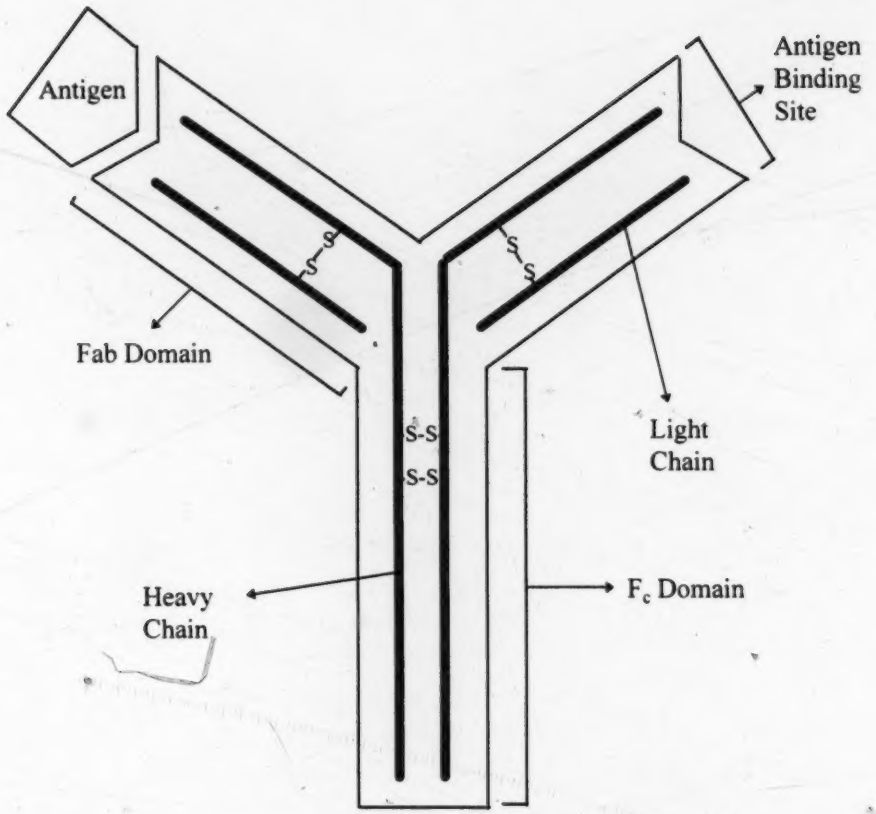

Figure 1-5 Basic Structure of an Antibody Molecule

Fab and the F_c domains may be cleaved using pepsin or papain to produce independent Fab and F_c fractions. Using pepsin, cleavage occurs along the F_c domain between the two di-sulphide bonds to produce an F_c fragment where the two heavy chains are connected by one di-sulphide bond and a Fab fraction where the two arms of the Y are linked by one di-sulphide bond. In this case, the Fab fragment is referred to as $F(ab')_2$. Using papain, cleavage occurs such that the two di-sulphide bonds in the F_c domain remain with the F_c fragment. This cleavage results in two separate Fab fragments. The following equation represents the two types of cleavage of antibodies.

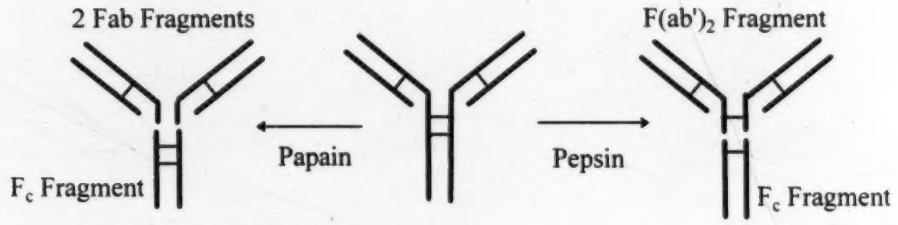

The IgG antibody molecule has a molecular weight of about 150 000 Daltons. With papain cleavage, the two Fab fragments and the F_c fragment are approximately 50 000 Daltons each. In the case of pepsin cleavage, the $F(ab')_2$ fragment is 102 000 Daltons and the F_c portion is about 48 000 Daltons.

1.4.3 Antibody-Antigen Interaction

Antibodies bind to antigens for which they have a specificity. The strength of the antibody-antigen interaction is called affinity and the stability of the complexes formed is referred to as avidity. The region of an antigen which binds to an antibody is termed an epitope. There are two types of antibodies used in immunoassays -

monoclonal and polyclonal antibodies. Monoclonal antibodies are specific for a single epitope. Polyclonal antibodies have the ability to bind to several epitopes on a single antigen. Antibodies are so highly specific that slight modification in the epitope structure may prevent recognition.

Antibody-antigen binding occurs through non-covalent interactions which include van der Waals forces, hydrogen bonds, coulombic interactions and hydrophobic bonds. In some cases antibody-antigen complexation may be accompanied by large structural changes in the antibody or antigen. Antibody-antigen interactions are reversible and the affinity constant, K_a = [Ab-Ag] / [Ab] [Ag], predicts the amount of antibody-antigen complex that will be present at equilibrium. The affinity constant is affected by pH, temperature and solvent which may shift the equilibrium forwards or backwards. Monoclonal antibodies are homogeneous and hence their affinities may be determined exactly. However, since polyclonal antibodies are comprised of several antibodies with different affinities, the exact affinity constant cannot be determined.

Three primary factors determine the thermodynamic strength and kinetic stability of an antibody-antigen complex. These are the affinity of the antibody for the epitope, the valency and the geometric arrangement of the antibody and antigen. Formation of multivalent complexes greatly increases the avidity of the complex. This can occur when either the antibody or the antigen or both are multivalent. Antibodies are multivalent. Antigens are multivalent if they contain several copies of the same epitope or if they contain several epitopes which are recognized by different antibodies. Multivalent binding of antibody to antigen can result in large, stable, multimeric complexes. However, this may be affected by the geometric arrangement of the antibody and antigen and whether they cause steric hindrances.

1.5 Summary

Use of chemiluminescence detection in microchip capillary electrophoresis and its application to immunoassays is demonstrated in this thesis. The horseradish peroxidase catalyzed reaction of luminol and hydrogen peroxide is used for this purpose. Horseradish peroxidase or a protein conjugated to horseradish peroxidase is used as sample. Luminol is added to the separation buffer and hydrogen peroxide is introduced in post separation manner. Optimization of luminol and hydrogen peroxide concentrations, as well as pH is done. A detection limit study is conducted using horseradish peroxidase, fluorescein conjugated. Also, an immunoassay reaction is demonstrated using $F(ab')_2$ fragment goat anti-mouse IgG, HRP conjugate directed against mouse IgG whole molecule.

In Chapter 2, the optimization of luminol and hydrogen peroxide concentrations, as well as pH studies is discussed. This is necessary in order to obtain maximum signal from the system. A detection limit study of a horseradish peroxidase conjugate is presented in Chapter 3. This is done to evaluate the potential of the detection scheme using microchip capillary electrophoresis. In order to demonstrate that chemiluminescence detection can be applied to analytically useful reactions, immunoassays were conducted using this detection scheme. Chapter 4 describes the application of chemiluminescence detection for immunoassays, using microchip CE. Finally conclusions and future directions are presented in Chapter 5.

1.6 References

(1) Harrison, D. J.; Manz, A.; Fan, Z.; Ludi, H.; Widmer, H. M. *Anal. Chem.* **1993,** *64*, 1926.

(2) Manz, A.; Harrison, D. J.; Verpoorte, E. M. J.; Fettinger, J. C.; Paulus, A.; Ludi, H.; Widmer, H. M. *J. Chromatogr.* **1992,** *593*, 253.

(3) Effenhauser, C. S.; Manz, A.; Widmer, H. M. *Anal. Chem.* **1993,** *65*, 2637-2642.

(4) Harrison, D. J.; Seiler, K.; Manz, A. *Anal. Chem.* **1993,** *65*, 1481-1488.

(5) Harrison, D. J.; Fluri, K.; Seiler, K.; Fan, Z.; Effenhauser, C. S.; Manz, A. *Science* **1993,** *261*, 895-897.

(6) Harrison, D. J.; Fan, Z. H. *Anal. Chem.* **1994,** *66*, 177-184.

(7) Harrison, D. J.; Seiler, K.; Fan, Z. H.; Fluri, K. *Anal. Chem.* **1994,** *66*, 3485-3491.

(8) Campana, A. M. G.; Baeyens, W. R. G.; Zhao, Y. N. *Anal. Chem.* **1997,** *69*, A83-A88.

(9) Staller, T. D.; Sepaniak, M. J. *Instrumentation Science & Technology* **1995,** *23*, 235-254.

(10) Harrison, D. J.; Chiem, N. *Anal. Chem.* **1997, *69***, 373-378.

(11) Lukas, K. D.; Jorgenson, J. *Anal. Chem.* **1981,** *53*, 1298-1302.

(12) Lukas, K. D.; Jorgenson, J. *Science* **1983,** *222*, 266-272.

(13) Lukas, K. D.; Jorgenson, J. *J. HRC &CC* **1985,** *8*, 407-411.

(14) Chien, R.; Burgi, D. S. *Anal. Chem.* **1992,** *64*, 489A-496A.

(15) Cooksy, K. In *The Separation Times*, 1993; Vol. 7.

(16) Lee, C. S. In *Handbook of Capillary Electrophoresis*; Landers, J. P., Ed.; CRC Press, 1997.

(17) Ewing, A.; Wallingford, R. A.; Olefirowicz, T. M. *Anal. Chem.* **1989,** *61*, 292A-303A.

(18) Fan, Z. H. PhD, University of Alberta, 1994.

(19) Bowie, A. R.; Sanders, M. G.; Worsfold, P. J. *J. Biolumin. Chemilumin.* **1996,** *11*, 61-90.

(20) Rongen, H. A. H.; Hoetelmans, R. M. W.; Bult, A.; Van Bennekom, W. P. *J. Pharm. Biomed. Anal.* **1994,** *12*, 433-462.

(21) McCapra, F.; Gunderman, K. D. *Chemiluminescence in Organic Chemistry*; Springer-Verlag Berlin Heidelberg: Germany, 1987.

(22) Quina, F. H. *Photophysical Concepts in Condensed Media*; Academic Press: London, 1982.

(23) Nieman, T. A. In *Encyclopedia of Analytical Science*; Townshend, A., Ed.; Academic Press, 1995; Vol. 1, pp 608-621.

(24) White, E. H.; Roswell, D. F. In *Chemi- and Bioluminescence*; Burr, J. G., Ed.; Marcel Dekker, Inc: New York, 1985.

(25) Albrecht, H. O. *Z. Phys. Chem.* **1928,** *136*, 321-330.

(26) Easton, P. M.; Simmonds, A. C.; Rakishev, A.; Egorov, A. M.; Candeias, L. P. *J. Am. Chem. Soc.* **1996,** *118*, 6619-6624.

(27) Sanchez, F. G.; Diaz, A. N.; Garcia, J. A. G. *Journal Of Luminescence* **1995,** *65*, 33-39.

(28) Kricka, L. J.; Ji, X. *J. Biolumin. Chemilumin.* **1995,** *10*, 49-54.

(29) Diaz, A. N.; Sanchez, F. G.; Garcia, J. A. G. *Journal Of Photochemistry And Photobiology A Chemistry* **1995,** *87*, 99-103.

(30) Diaz, A. N.; Sanchez, F. G.; Garcia, J. A. G. *Analytica Chimica Acta* **1996,** *327*, 161-165.

(31) Diaz, A. N.; Sanchez, F. G.; Lovillo, J.; Garcia, J. A. G. *Analytica Chimica Acta* **1996,** *321*, 219-224.

(32) Kennedy, R. T.; Schultz, N. M. *Anal. Chem.* **1993,** *65*, 3161-3165.

(33) Karger, B. L.; Shimura, K. *Anal. Chem.* **1994,** *66*, 9-15.

(34) Chen, F. T. A.; Pentoney, S. L. *J. Chromatogr. A* **1994,** *680*, 425-430.

(35) Chen, F. T. A. *J. Chromatogr. A* **1994,** *680*, 419-423.

(36) Harlow, E.; Lane, D. *Antibodies A Laboratory Manual*; Cold Spring Harbor: New York, 1988.

CHAPTER 2

OPTIMIZATION OF CHEMILUMINESCENT REACTION

2.1 Introduction

Use of chemiluminescence as a method of detection for microchip capillary electrophoresis devices is demonstrated. Several chemiluminescent reactions were tried in bulk solution to determine which ones were most suitable for use on the chip. This led to the horseradish peroxidase catalyzed reaction of luminol and hydrogen peroxide being chosen for further work. This required optimization of reaction conditions on-chip in order to obtain maximum emission. The concentrations of luminol and hydrogen peroxide were optimized, as well as the reaction pH. Optimum conditions were obtained by studying concentration of luminol in the range 1-10 mM and hydrogen peroxide from 0.3-3.0 %. pH was studied in the range 8.0-10.5.

Luminol and hydrogen peroxide (H_2O_2) concentration studies were conducted using both horseradish peroxidase (HRP) and horseradish peroxidase fluorescein conjugated (HRP-Fl). The conjugate of HRP was studied because the system was being developed for the detection of antibodies or antigens labeled with HRP. Therefore, it was important to observe the responses of HRP conjugates. The response for luminol and H_2O_2 were similar for both HRP and HRP-Fl. The results for luminol with HRP and HRP-Fl are presented to show the similarities in trend. For H_2O_2 and pH studies only the data with HRP-Fl is presented.

2.2 Experimental

2.2.1 Device Fabrication

The layouts of the two devices used are illustrated in Figure 2-1. Both devices incorporated a double-T injector similar to that reported by Effenhauser, et al.,[1] as well as a Y-shaped intersection allowing for the post separation addition of reagents. In device PCRD 1, there was a 90° turn about 100 μm after the Y intersection, whereas with PCRD 2 the turn was 0.75 cm after the intersection. In addition, the width of the channel after the mixing intersection was twice that of the feed channels for PCRD 2 (not illustrated in Figure 2-1) but the same for PCRD 1.[2] The length from the separation buffer reservoir to the Y mixing point was 5.9 cm for PCRD 1 and 5.05 cm for PCRD 2. From the injector to the Y intersection, the distance was 4.55 cm for PCRD 1 and 3.8 cm for PCRD 2. From the post column reservoir to the Y intersection, the distance was 3.25 cm for PCRD 1 and 2.55 cm for PCRD 2. The channels were 12-15 μm deep in both devices and the double-T injector was 100 μm in length. The thin lines illustrated in Figure 2-1 represent channels with a width of 30μm and the thick lines indicate regions that are 240 μm wide.

Devices were fabricated in 3" square Corning Pyrex 7740 glass (Paragon Optical Co., PA) by the Alberta Microelectronic Center (AMC) using modifications of bulk silicon micromachining methods.[3] Devices consisted of two pieces of 1.95 mm thick glass; one with etched channels and the other with drilled access holes, thermally bonded together. Figure 2-2 illustrates the main steps in the etching process.

Glass plates were either thermally annealed or used as received. The plates were then cleaned in detergent, methanol, acetone and deionized water in an

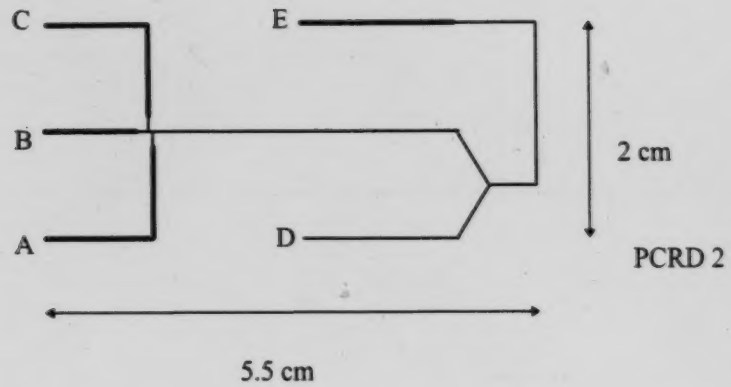

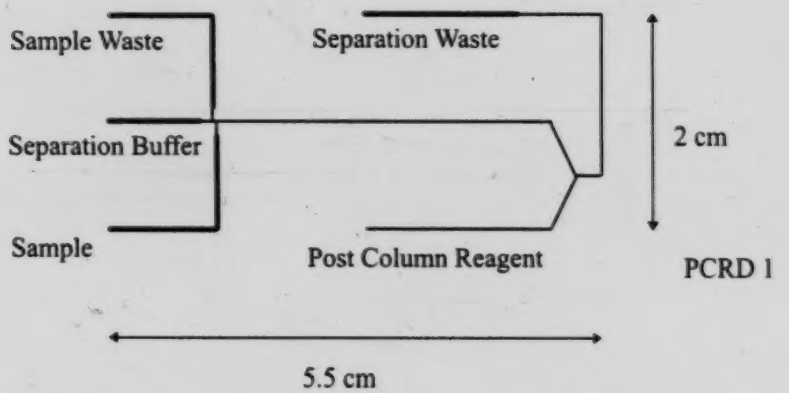

Figure 2-1 Layout of Devices PCRD 1 and 2. The thin lines represent channels with a width of 30 μm and the thick lines indicate regions that are 240 μm wide. The corresponding labels on both devices are equivalent and may be used interchangeably.

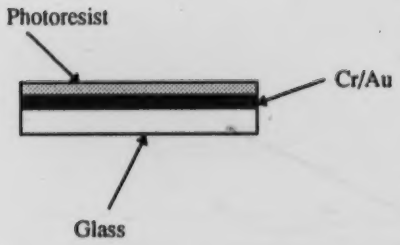

Stage 1 - The glass is coated with a layer of Cr/Au followed by a layer of photoresist

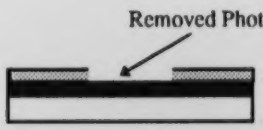

Stage 2 - The photoresist is exposed to UV light thereby removing the desired regions

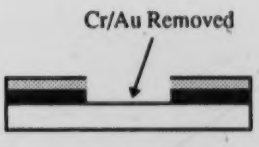

Stage 3 - The exposed Cr/Au layer is removed using commercial Cr etch and aqua regia

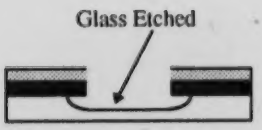

Stage 4 - The exposed glass is etched using $HF/HNO_3/H_2O$

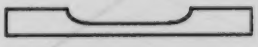

Stage 5 - The remaining photoresist and Cr/Au layers are stripped

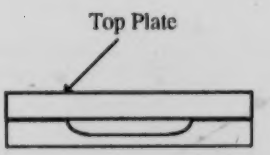

Stage 6 - The top plate with drilled access holes is thermally bonded to the etched plate

Figure 2-2 Diagram Illustrating the Main Fabrication Steps for Microchips

ultrasonic bath under a class 100 clean hood. A Cr/Au metal layer was first deposited on the cleaned glass surface followed by a layer of photoresist. Using a mask, the desired regions of the photoresist were exposed to UV light and developed, thereby removing those regions. The exposed metal layer was etched away with commercial Cr etch and aqua regia. Using $HF/HNO_3/H_2O$ (20:14:16) etchant, the exposed glass layer was etched 10-15 μm deep to produce microchannels. The remaining photoresist and Cr/Au layers were then stripped using the methods stated previously.

The etched wafer formed the bottom plate of the device. The top plate had 1·9 mm diameter holes drilled into it, to provide access to the channels. Both top and bottom plates were cleaned by immersing in H_2SO_4/H_2O_2 (3:1) for 20-30 minutes, then washed in a class 100 clean hood using a MicroAutomation 2066 High Pressure Cleaning Station. The two plates were then aligned and contacted. Manual pressure was applied to remove trapped air. The absence of interference fringes indicated good contact. The presence of small particles resulted in Newton's rings surrounding the contaminant. If the rings intersected the channels, the plates were separated and pressure washed again. Once all areas of the channels were completely contacted, permanent bonding was done using the program listed in Table 2-1. The microchips were completed by attaching solution reservoirs. These were eppendorf pipette tips cut to about 1 cm sizes and inserted in the drilled holes of the top plate.

STAGE	1	2	3	4
RATE (°C/MIN)	10	10	10	5
TEMP (°C)	550	610	635	650
TIME (HRS)	0.5	0.5	0.5	6.0

Table 2-1 Pyrex Bonding Temperature Program

2.2.2 Instrumentation

A schematic diagram illustrating the instrument setup is shown in Figure 2-3. The chip was held on a specially designed Plexiglas block holder that had electrical connection to the power supplies through high voltage relays. Connections to the solution reservoirs were made by means of platinum wires attached to the outlets on the chip holder. The chip holder was seated on an x-y translation stage. A microscope objective and tube were located directly above the chip. The photomultiplier tube was placed on top of the microscope tube. The entire optical setup was enclosed in a light tight black box.

Solution manipulation on chip was achieved using a computer controlled power supply (-3 and -15 kV MJ series, Glassman High Voltage, Whitehouse Station, NJ and a Spellman Model CZE 1000R power supply, Plainview, NY) and relay system using programs written in Labview (National Instruments Corp., Austin, TX).[2, 3] Injection was done by applying ground at A (sample) and B (separation or inlet buffer) and a negative potential to C (sample waste), thus effecting solution flow from A and B to C across the double-T injector. During injection D and E were disconnected, i.e. the relays were open. After the specified injection time elapsed, A and C were disconnected and D (post column or separation reagent) and E (separation or outlet waste) connected simultaneously for separation. A negative voltage was applied at E while D floated at some negative potential higher than ground but lower than E. Hence solution flowed from B and D to E.

Chemiluminescent light generated about 0.1-1.0 mm after the Y mixing intersection was collected by a 25X Leitz Fluotar (0.35 N.A.) objective and directed through a 450 nm (±10 nm) optical bandpass filter (Omega Optical, Brattleboro, VT) into a Hamamatsu photomultiplier tube. The PMT current was converted to a voltage

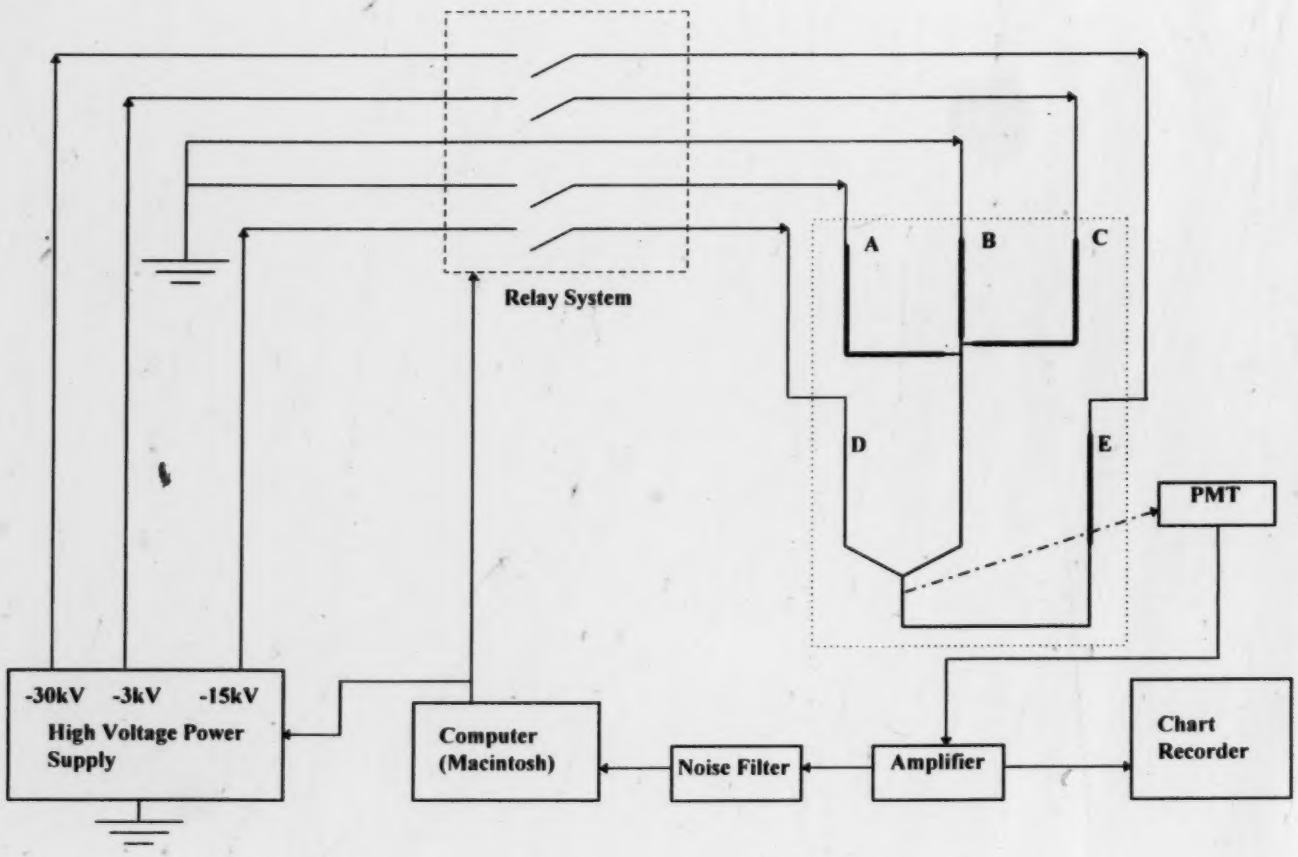

Figure 2-3 Diagram Illustrating the Instrumental Set-Up

and amplified using a 10^8 Ω impedance amplifier. The signal was then routed in two directions; one to a Fisher Recordall Series 5000 chart recorder and the other through a 25 Hz noise filter to a Macintosh Centris 650 computer. The National Instruments A/D board sampling rate was 100 Hz.

2.2.3 Materials

Borate buffer was prepared by dissolving either 10 or 100 mM boric acid (J.T.Baker, Phillipsburg, NJ) in doubly distilled de-ionized water and adjusting to the required pH using 1M NaOH (BDH). Reagents were used as received. Horseradish peroxidase Type IV A (HRP), fluorescein (Fl) and 5-amino-2,3-dihydro-1,4-phthalazinedione (luminol) were purchased from Sigma (St. Louis, MO). Horseradish peroxidase fluorescein conjugate (HRP-Fl) came from Molecular Probes (Eugene, OR) and hydrogen peroxide (H_2O_2) was from Caledon (Georgetown, ON). Solutions of luminol, HRP, Fl and HRP-Fl were prepared by dissolving the required amounts of reagent in buffer. Luminol required extensive vortexing using a Vortex-2 Genie to ensure complete dissolution.

HRP, Fl and HRP-Fl solutions were stored protected from light at 4 °C. Luminol was stored at room temperature protected from light. The hydrogen peroxide reagent was stored in the refrigerator. Solutions of H_2O_2 used on chip were prepared fresh each day by diluting the 30 % reagent to the required concentration in running buffer.

All solutions used on the chip were filtered through 0.22 μm pore filters. Protein solutions, luminol and hydrogen peroxide were filtered using cellulose acetate syringe filters from either Millipore (Bedford, MA) or Nalge Co. (Rochester, NY).

Buffers were filtered through nylon syringe filters from Micron Separations Inc. (Westboro, MA). Small volumes of HRP-Fl sample were filtered using 0.22 μm size Micropore Separators (Amicon, Beverly, MA) and a micro-centrifuge in order to minimize solution retention on the filters.

2.24 Procedures

Each day before the start of experiments the chip was flushed with 1 M NaOH for 10 minutes, water for 10 minutes and buffer for 30 minutes using vacuum. Solution flows were checked by testing for stable currents. Two simple tests were carried out. With buffers in all reservoirs, ground potential was applied at reservoirs A and B and -5 kV at E. Stable currents indicated good flow. Similarly, currents were monitored with ground applied at C and D and -5 kV at E. Unstable currents necessitated flushing for another 30 minutes with buffer. This was followed by the optimization of the signal.

Sample was placed in reservoir A, luminol in B and H_2O_2 in D. Reservoirs C and E contained buffer. Ground potential was applied at A and B with D floating and E at -5 kV. This produced a continuous stream of chemiluminescent product flowing past the detector. The signal was recorded on a chart recorder. The position at which emission was maximum was obtained by translating the chip in the x and y direction and the microscope in the z direction individually until optimum signal was attained. Usually the optimum occurs in a region 0.1-1.0 mm from the Y intersection. The field of view of the lens was 0.7 mm diameter. After optimization, experiments were conducted. At the end of each day's experiment the chip was flushed with water for 10 minutes followed by 1 M NaOH for 10 minutes and then again with water for 10 minutes. The chip was then stored wet with water.

2.3 Results and Discussion

2.3.1 Preliminary Chemiluminescent Reactions

Preliminary study of chemiluminescent reactions resulted in the following systems being selected for trials in bulk solution.

Table 2-2 Chemiluminescent Reactions Studied

CL Reagent	Catalyst	Ox Agent	Buffer	pH
fluorescein	HRP[a]	H_2O_2	MOPS-NaOH[b]	7.0
luminol	HRP	H_2O_2	tris	8.0
luminol	$K_3Fe(CN)_6$	H_2O_2	borate	10.5
MAN[c]		H_2O_2	borate	
luminol	MP[d]	H_2O_2	borate	9.5

[a] horseradish peroxidase, [b] (3-(N-morpholinopropane)sulphonic acid)-NaOH, [c] methyl acridinium nitrate, [d] microperoxidase

The fluorescein (Fl)/horseradish peroxidase (HRP)/hydrogen peroxide (H_2O_2) reaction in (3-(N-morpholinopropane)sulphonic acid)-NaOH (MOPS-NaOH) buffer at pH 7.0 published by Segawa, Kamidate and Watanabe[4] was replicated. The exact concentrations and proportions of reagents stated in the article were used. Chemiluminescent emission was observed visually in a dark room, instead of using a luminometer. However, no light emission could be seen. Unfortunately, we could not explain this behaviour.

The luminol/HRP/H_2O_2 reaction was conducted in tris buffer at pH 8.0. [5] The reaction resulted in a faint blue light emission. The reaction was also attempted at pH 7.4 in phosphate buffer with no luminescence, indicating the importance of pH in the luminol/HRP/H_2O_2 system.[6, 7] The luminol/$K_3Fe(CN)_6$/H_2O_2[7, 8] reaction was conducted successfully at a high pH of 10.5.

Methyl acridinium nitrate (MAN)/H_2O_2[7] requires no catalyst, but a high pH is needed. Acridinium esters undergo reversible conversion to the non-chemiluminescent pseudo-base form in alkaline solution. Hence, the literature states that it has to be reconverted to the acidic acridinium ester followed by the addition of NaOH to initiate chemiluminescence. The methyl acridinium nitrate was dissolved in doubly distilled deionized water instead of buffer. Using pH paper, the pH of this solution was tested and found to be approximately 5-6. H_2O_2 was diluted in pH 10.5 borate buffer and the pH of this solution was found to be about 8. Adding H_2O_2 to methyl acridinium nitrate did not yield chemiluminescence. However, adding a few drops of NaOH triggered emission. The pH of this final solution was tested with pH paper and found to be approximately 9-10. Apparently, this preparation procedure ensures at least some acidic acridinium is present.

The luminol/microperoxidase (MP)/H_2O_2 experiment was a modification of the work published by Zhao, Labbe and Dovichi.[9] We used luminol instead of isoluminol as used by those authors. The reaction was quite successful. Visually, it was noted that the chemiluminescence decayed rapidly compared to the other systems tried, following mixing of reagents. This reaction was promising and initial trials were performed on chip. Unfortunately, reproducible peak injection heights were possible only if the enzyme solution was replaced every 5-7 injections.

2.3.2 On-Chip Experiments

The horseradish peroxidase (HRP) catalyzed reaction of luminol and hydrogen peroxide (H_2O_2) was chosen for further work. The methyl acridinium nitrate reaction was a bit complicated since it required conversion to the acidic form followed by addition of highly basic reagent to be successful. The luminol/ferricyanide reaction also required very basic pH. In addition, we had difficulties driving the negatively charged ferricyanide ion in the right direction on-chip using electrokinetic pumping. Also, as discussed before we had reproducibility problems with the luminol/MP system. Hence, the luminol/HRP/H_2O_2 system, which required moderate pH, seemed to be the most suitable choice. Moderate pH was preferred in order to avoid possible denaturation of the protein. In addition, high pH was undesirable since it could modify the surface properties of the glass device over long periods of exposure.

It was necessary to mix all reagents on chip, as discussed below. For obvious reasons the luminol, HRP and H_2O_2 could not be pre-mixed. Pre-mixing two of the reagents and adding the third on-column was not an option either. HRP and H_2O_2 could not be mixed since H_2O_2 would destroy the enzyme. HRP and luminol or H_2O_2 and luminol could not be mixed because electrogenerated chemiluminescence occurred at the electrodes when a voltage was applied. Therefore, all reagents were introduced as separate streams and mixed on chip. HRP was used as sample, luminol was present in the separation buffer and H_2O_2 was in the post separation reservoir. Optimum conditions were obtained by studying pH in the range 8.0-10.5, concentration of luminol from 1-10 mM and concentration of hydrogen peroxide from 0.3 - 3.0 %.

The initial assumptions were that the concentrations of luminol and hydrogen peroxide should be in excess so that the concentration of HRP is limiting, since it is

the protein we ultimately want to detect. The first experiments on-chip were done in a continuous flow mode using either vacuum or electrokinetic pumping to determine whether it was possible to detect chemiluminescent light in the microchannels. Using 25 μM HRP as sample with 20 mM luminol in the inlet buffer and 3 % H_2O_2 in the post column reservoir, a vacuum was applied at the outlet. 10 mM borate buffer, pH 10.5 was present in the sample waste and separation waste reservoirs. For electrokinetic pumping, ground potential was applied simultaneously to the sample, inlet buffer and post column reservoirs and -5 kV at the outlet. Both pumping methods effected solution flow of HRP, luminol and H_2O_2 towards the outlet.

Chemiluminescent light was detected shortly after the Y-mixing intersection both visually and by light collection with a photomultiplier tube. This confirmed the possibility of detecting chemiluminescent light in microchannels. Hence, injections and separations were carried out by injecting a plug of 25 μM HRP and separating with 20 mM luminol present in the separation buffer. The separation did not seem to be affected by the luminol present in the separation buffer as there was no increase in background nor was there any obvious peak distortions. Hydrogen peroxide (3 %) was added in a post column manner generating chemiluminescence with the HRP/luminol plug, which was detected as a single peak.

2.3.3 Sample Leakage

During the initial separation studies, sample leakage was observed. This was indicated by the high baseline present during separation. Figure 2-4 illustrates the baseline shift observed due to leakage. The leakage phenomenon was confirmed by injecting and separating a 5 μM fluorescein solution prepared in running buffer. The running buffer used was 10 mM borate at pH 10.5. A 488 nm Argon ion laser (Uniphase 2014, San Jose, CA) was used for excitation of the injected plug. The

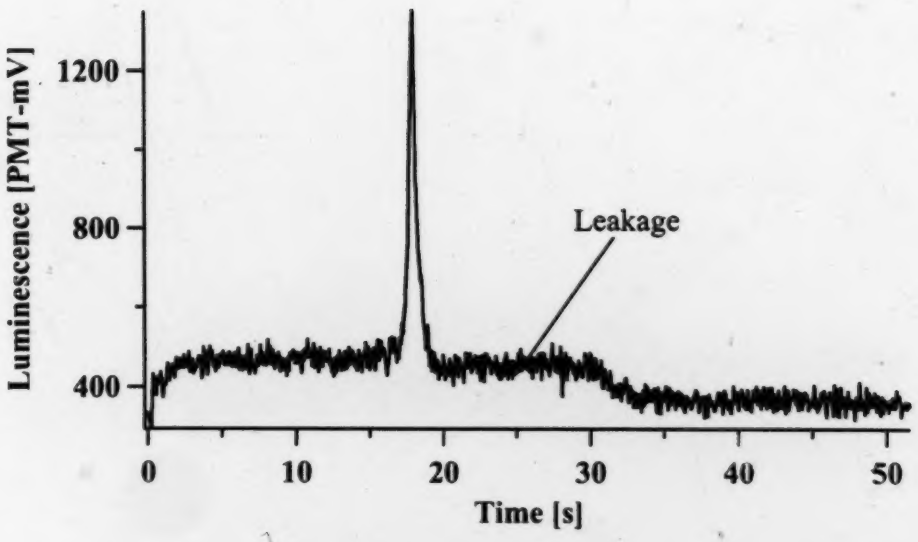

Figure 2-4 Electropherogram Showing Leakage During Separation

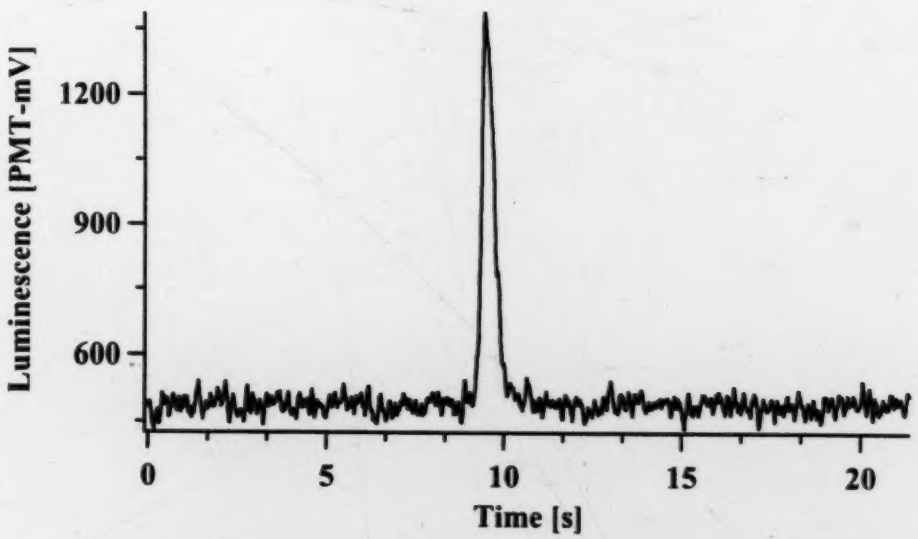

Figure 2-5 Electropherogram Showing No Leakage

injection/separation processes taking place at the double-T injector were observed visually. These experiments revealed sample leakage from both the sample and sample waste channels into the main channel during separation. This leakage phenomenon was prevented by adjusting the solution levels in the sample and sample waste reservoirs to be lower than the separation buffer reservoir. This was done in order to have a hydrostatic pushback of solution into the side channels during separation. The results obtained while there was no leakage is illustrated in Figure 2-5.

2.3.4 Luminol Optimization

For the luminol concentration study, both HRP and HRP-Fl data are presented. For HRP, 1, 2, 5 and 10 mM luminol were present in the separation buffer. The concentration of HRP and H_2O_2 were fixed at 25 μM and 3 % respectively. The running buffer used was 10 mM borate at pH 10.5. The PMT was set at 835 V. A sample of HRP was injected by applying ground potential at reservoirs A and B and -1.2 kV at C for 30 s. Separation was achieved by applying ground at B and -6 kV at E with D floating. The data obtained is illustrated in Figure 2-6. Each data point reflects the average peak height for five injections and the error bars indicate the standard deviation.

In a similar study with HRP-Fl, the protein concentration was fixed at 2.2 mg/ml (50 μM) and H_2O_2 at 1.5%. It should be noted that the concentration of HRP-Fl used was twice that of HRP. This was because the enzyme activity of HRP was 254 units/mg whereas the activity of HRP-Fl was 100-150 units/mg, as specified by the supplier. We tried to use solutions with similar activity, hence the concentration difference. 1, 2, 5 and 10 mM luminol were used in the separation

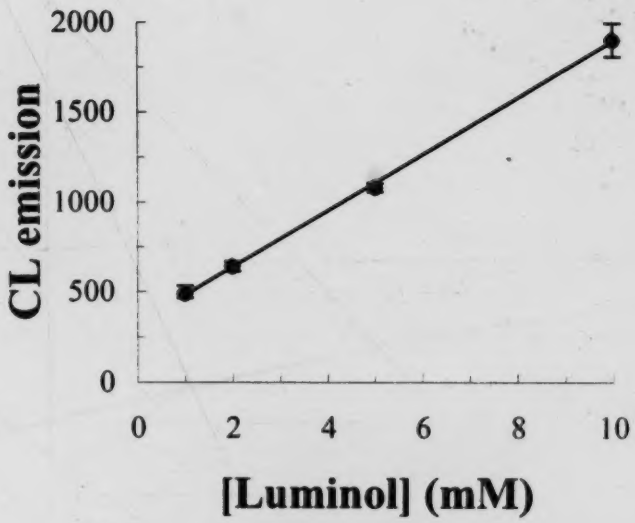

Figure 2-6 Chemiluminescent Response to Luminol Concentration Using HRP

buffer; 10 mM borate, pH 10.5. A plug of HRP-Fl was injected by applying ground at the sample and inlet buffer and -1.2 kV at the sample waste for 30 s. Separation was effected by applying ground at the inlet buffer and -6 kV at the outlet with the post column reservoir floating. The PMT voltage was set at 835 V. The results obtained are displayed in Figure 2-7. Each data point represents the average peak height for five consecutive injections. The error bars reflect one standard deviation.

Both HRP and HRP-Fl show linear responses (R^2 = 0.9995 and 0.9837 for HRP and HRP-Fl respectively) to luminol concentrations. However, the slopes are different and non-zero intercepts are seen. The expected curve over a large range of luminol concentrations is one that is linear at low concentrations with zero intercept, but begins to plateau at higher concentrations. The sharper gradient of the HRP curve seems to indicate that we are in the linear region of the luminol curve. However, the more gentle gradient observed for HRP-Fl suggests we are in the region where the luminol curve is beginning to plateau. This is in agreement with the R^2 values obtained for the two plots, meaning that the linear fit for HRP-Fl was not as good as that for HRP. It seems as though with the conjugated form of HRP a plateau is reached much earlier than with native HRP. This may be indicative of loss in HRP activity due to conjugation, consistent with the lower activity per milligram of conjugated protein.

A working concentration of 5 mM luminol was chosen based on the above results. Even though 5 mM gave less than maximum emission, it was chosen for several reasons. Firstly, luminol is very difficult to dissolve, hence, lower concentrations are more easily prepared. Second, luminol seems to undergo an oxidation reaction at the platinum electrode which results in a brown/black powdery coating forming at the electrode that comes off and floats in the solution. This material eventually finds its way into the channels, leading to blockages. Finally, there is a risk of concentrated luminol precipitating during chemiluminescent

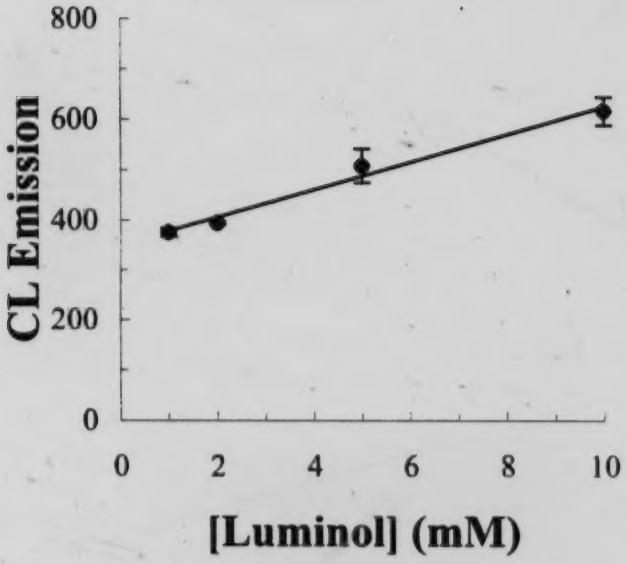

Figure 2-7 Chemiluminescence Response to Luminol Concentration Using HRP-Fl

reaction, resulting in blockages as well. Using lower concentrations reduced these risks.

2.3.5 Hydrogen Peroxide Concentration Study

The H_2O_2 concentration was optimized with the concentration of HRP-Fl fixed at 2.2 mg/ml and luminol at 5 mM. HRP-Fl was injected for 30 s at -1.2 kV; -6 kV was applied for separation. 0.3, 0.6, 1.5 and 3 % H_2O_2 were added from the post separation reservoir as previously described. The running buffer used was 10 mM borate, pH 10.5 and the PMT was set at 835 V. The results obtained are shown in Figure 2-8. Each data point reflects the average peak height of five consecutive injections and the error bar displays the standard deviation.

The results obtained are in partial agreement with the literature. According to O. Ryan, M. R. Smyth and C. O. Fagain,[10] low concentrations of H_2O_2 decrease HRP activity whereas high concentrations result in substrate inhibition. However, the authors report a 0.1 mM-2 mM optimum concentration range of H_2O_2. This does not agree with the concentration range of our study. Our range; 0.3-3.0 % corresponds to 0.1-1.0 M.

There was almost no change in signal between 1.5 and 3.0 %. However, the lower value of 1.5 % was chosen as a working concentration. This was due to hydrogen peroxide's tendency to form bubbles which can pose serious problems if they enter the channels. Bubbles result in unstable baselines and fluctuating signals.

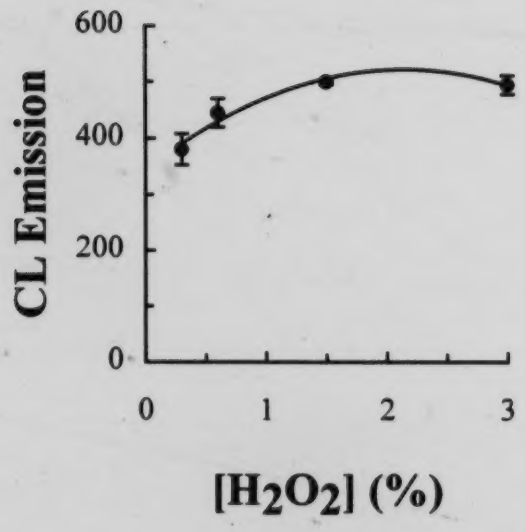

Figure 2-8 Chemiluminescence Response to Hydrogen Peroxide Concentration Using HRP-Fl

2.3.6 Response to pH

Optimization of pH was done by studying the range between 8.0 and 10.5 in 0.5 increments. 100 mM borate buffers were prepared at pH's 8.0, 8.5, 9.0, 9.5, 10.0 and 10.5 by dissolving boric acid in doubly distilled deionized water and adjusting to the required pH with 1M NaOH. For these studies, 88 μg/ml HRP-Fl, 5 mM luminol and 1.5 % H_2O_2 used were all prepared in the desired buffer. Experiments were conducted at each pH by injecting a plug of HRP-Fl at -1.2 kV for 30 s and subsequently applying -6 kV for separation. Maximum emission occurred at pH 9.0. The results obtained are plotted in Figure 2-9. Each data point indicates the average peak area of five consecutive injections at each pH. The standard deviation is reflected by the error bar. Figure 2-10 shows a plot of the peak areas at each pH normalized for EOF changes by dividing by their respective migration times. In this case, maximum emission was observed at pH 8.5.

This pH study indicates that the maximum chemiluminescent emission occurs around pH 8.5-9.0. According to the Encyclopedia of Analytical Science,[7] maximum emission for the luminol/HRP/H_2O_2 system occurs in the range pH 7-9.5 with an optimum around pH 8.5. "It is a compromise between loss of HRP activity at higher pH and loss of luminol chemiluminescence at lower pH." Also, in an article published by W. Sun, X. Ji, L. J. Kricka and B. Dunford,[6] they propose that at low pH, luminescence is low even though HRP is in its reactive protonated state. This is due to luminol intensity being weak at low pH. At high pH luminol luminescence is strongest, however, HRP is in its unreactive deprotonated state. Therefore, luminescence is also low at high pH. Optimum conditions occur around pH 8.6 since HRP is still reactive and luminol emits reasonably well at this pH. Hence, our results are in agreement with the literature.

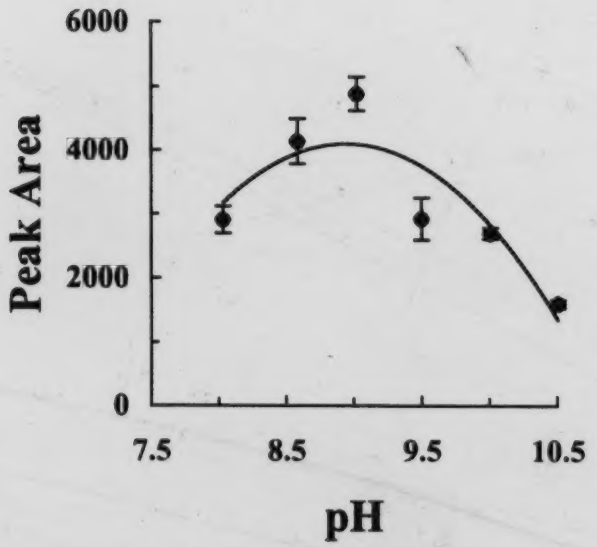

Figure 2-9 Chemiluminescence Response to pH

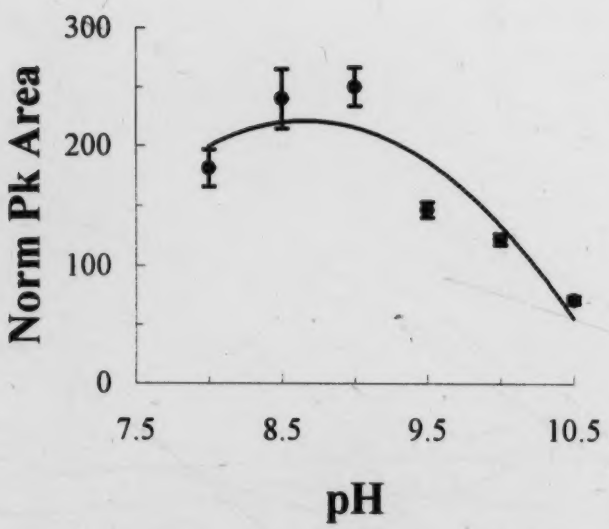

Figure 2-10 Normalized Peak Area for the Chemiluminescence Response to pH

2.4 Conclusions

Our preliminary study of chemiluminescent reactions proved to be quite useful in determining which reactions were most suitable for use on-chip. Highly basic reaction systems were unsuitable because of the possibility of modifying the surface of the microchannels over long periods of exposure. In addition, high pH may cause denaturation of the protein which may have adverse effects on the reaction. Acidic and basic conditions mixed on-chip were not desirable either. Different flow behaviours would be expected in the acidic and basic regions of the chip resulting in irreproducible results. This eliminated the acridinium system. Hence, our choice of chemiluminescent systems reduced to either the HRP or MP catalyzed reaction of luminol and H_2O_2. We chose HRP over MP since it gave more stable results.

Optimization of concentrations and pH also proved to be beneficial. We were able to compare our results to the literature to determine whether the responses on-chip were similar to those reported. The optimum pH seemed to be in agreement with the literature. However, the H_2O_2 concentration obtained was different from that reported by Smyth et. al.[10] We believe that this was because our measurements were made in flowing streams for a few seconds and not integrated over a long time, in stationary solution systems. It is suspected that even though the high peroxide concentration may inactivate the enzyme, it immediately resulted in a burst of chemiluminescence which decayed fairly rapidly, probably due to enzyme inactivation. Since we do not integrate our signal over time, this was not a problem for us. The short burst of emission was to our advantage.

2.5 References

(1) Effenhauser, C. S.; Manz, A.; Widmer, H. M. *Anal. Chem.* **1993,** *65*, 2637-2642.

(2) Harrison, D. J.; Fluri, K.; Chiem, N.; Fitzpatrick, G. *Anal. Chem.* **1996,** *68*, 4285-4290.

(3) Harrison, D. J.; Fan, Z. H. *Anal. Chem.* **1994,** *66*, 177-184.

(4) Segawa, T.; Kamidate, T.; Watanabe, H. *Anal. Sci.* **1990,** *6*, 763-764.

(5) Prichard, P. M.; Cormier, M. J. *Biochem. Biophys. Res. Commun.* **1968,** *31*, 131-136.

(6) Sun, W.; Ji, X.; Kricka, L. J.; Dunford, H. B. *Can. J. Chem.* **1994,** *72*, 2159-2162.

(7) Nieman, T. A. In *Encyclopedia of Analytical Science*; Townshend, A., Ed.; Academic Press, 1995; Vol. 1, pp 608-621.

(8) Maeda, M.; Tsuji, A. *Analytica Chimica Acta* **1985,** *167*, 241-248.

(9) Zhao, J. Y.; Labbe, J.; Dovichi, N. J. *J. Microcolumn Sep.* **1993,** *5*, 331-339.

(10) Ryan, O.; Smyth, M. R.; Fagain, C. O. *Essays in Biochemistry* **1994,** *28*, 129-146.

CHAPTER 3

DETECTION LIMIT OF PEROXIDASE CONJUGATE

(Horseradish Peroxidase, Fluorescein Conjugated)

3.1 Introduction

In capillary electrophoresis, UV absorption detection is most popular. However, this detection system is not very sensitive, with levels of detection in the range 10^{-4} to 10^{-5} M.[1] Fluorescence and chemiluminescence detection schemes provide better detection limits, which may extend from 10^{-9} M down to 10^{-12} M or better. While fluorescence detection requires a light source, chemiluminescence does not. Therefore, chemiluminescence detection is usually referred to as a dark field technique. Since a source light is not required, there is no background from Rayleigh and Raman scattering, resulting in this detection method being inherently sensitive as well as simple. This makes it an ideal candidate for detection on microchips, since the overall system peripherals would be more compact, stable and portable. In this chapter we will present the results of a chemiluminescence detection limit study of HRP-Fl using the HRP/luminol/H_2O_2 system.

Although chemiluminescence detection gives low background signals and improved detection limits, it is subject to other limitations. Chemiluminescence lacks selectivity. In other words, any impurities in the sample or reagents with the ability to chemiluminesce will be detected. Also, optimum chemiluminescent emission may depend on several environmental factors such as pH, buffer additives, temperature

and ionic strength.[2, 3] Separation requirements may not coincide with these factors, leading to situations where the optimum chemiluminescent conditions have to be compromised. In addition, the chemiluminescent emission varies with time resulting in different intensities at various points after mixing. Therefore, it is important to determine the point at which the signal is maximum for detection.

In other work done using chemiluminescence detection in capillary electrophoresis, a variety of detection limits have been reported for various chemiluminescent systems. Hara, Nishida and Nakajima[4] reported a detection limit of 6 nM BSA labeled with tetramethylrhodamine isothiocyanate isomer R dye using the bis(trichlorophenyl) oxalate/H_2O_2 system. Their reaction was done in 50 μm i.d. capillaries and the injected volumes were about 20 nL. In another study by Zhao, Labbe and Dovichi[5], a detection limit of 20 nM was reported for isoluminol thiocarbamyl derivatives of amino acids using the isoluminol/MP/H_2O_2 system. This work was also done in 50 μm i.d. capillaries and their detection volume was 2 nL. In an ion analysis study conducted by Huang, Li, Zhang and Cheng[6] a detection limit of 500 fM was obtained for Co(II) using luminol and H_2O_2 reagents. The injected volume was 40 nL in a 50 μm i.d. stream, entering a 530 μm i.d. sheath flow capillary used in the detection region. Also, Zare, Dadoo and Colon reported detection limits of 3 nM and 7 nM for luminol and N-(4-aminobutyl)-N-ethylisoluminol (ABEI) which corresponds to 33 nL and 57 nL sample volumes respectively. 150 μm i.d. capillaries were used at the detection area for this work.

The above results are just a few of those published using chemiluminescence in the last few years. However, they give an indication of the kind of detection limits we needed to achieve in our system in order to become competitive. In some other work, higher detection limits were reported. These include 0.05 μM for BSA labeled with rhodamine B isothiocyanate and using the bis(trichlorophenyl) oxalate/H_2O_2

system,[7] 0.06 μM for BSA eosine Y complex using the bis(trichlorophenyl) oxalate/H_2O_2 system[8] and 0.2 μM for BSA using Rose Bengal with the bis(2.4.6-trichlorophenyl) oxalate/H_2O_2 system.[9]

We have achieved detection limits of HRP-Fl in the low nM region for the unenhanced reaction of luminol with H_2O_2, but, it was not possible without some amount of modifications to the chip operation and instrumental set-up. Our detection limits were calculated based on data obtained with a S/N < 20. We used this data and extrapolated linearly down to a concentration that would give a S/N of 3 and used that value as our detection limit. This chapter describes in detail all modifications made to our system and the results achieved.

3.2 Experimental

3.2.1 Device Fabrication

Devices were fabricated in 3" square, 1.95 mm thick Pyrex glass by the Alberta Microelectronic Center using the methods previously described in Chapter 2. The Pyrex plates used for etching the microchannels were either used as received or thermally annealed in order to eliminate glass defects. The top plates used for drilling the access holes were used as received. Bonding of the drilled top plate and etched bottom plate were done using the same cleaning and alignment procedure described earlier. This was followed by heat bonding and attachment of solution reservoirs.

3.2.2 Instrumentation

The instrumental set-up was identical to that presented earlier except for some modifications which are discussed later. Solution manipulation on-chip was also achieved in a similar manner as described in Chapter 2. A sample plug was injected by applying ground potential at the sample and separation buffer and a negative potential at the sample waste. Separation was achieved by applying ground to the separation buffer and a negative potential at the separation waste with the post column channel floating.

Chemiluminescent emission was collected by a 25X, 0.35 N.A. objective and directed into a PMT. The PMT current was converted into a voltage and amplified using a 10^8 Ω impedance amplifier. The signal was then recorded on a chart recorder. It was also filtered through a 25 Hz noise filter and recorded on a Macintosh computer. The A/D board sampling rate was 100 Hz.

3.2.3 Materials

Borate buffers were used in all experiments. For most of the early experiments 10 mM borate buffer pH 10.5 was used. However, later experiments were done using 100 mM borate containing 25 mM NaCl (BDH Inc., Toronto, ON) and 0.01 % w/v tween 20 (Sigma, St. Louis, MO) at pH 8.5.

Buffers were made by dissolving the required amounts of boric acid (J.T.Baker, Phillipsburg, NJ) and buffer additives (if used) in doubly distilled deionized water and adjusting to the desired pH using 1 M NaOH (BDH). All

reagents used on chip were prepared in the running buffer. 5 mM luminol (Sigma) and 1.5 % H_2O_2 (Caledon, Georgetown, ON) were used in all experiments. HRP-Fl (Sigma) was diluted each day from a 2 mg/ml stock solution. H_2O_2 was also prepared fresh each day by diluting from the 30 % reagent.

All solutions used on chip were filtered. Luminol and H_2O_2 were filtered using 0.22 μm cellulose acetate filters (Millipore, Bedford, MA). Buffers were filtered through 0.22 μm nylon syringe filters (Micron Separations Inc., Westboro, MA). To minimize solution retention on the filters, small volumes of HRP-Fl sample were filtered using 0.22 μm Micropore Separators (Amicon, Beverly, MA) and centrifuging.

3.2.4 Procedures

Each day before the start of experiments the device was cleaned using the procedure described in Chapter 2. Flows were checked by testing for stable currents and the device was aligned using x-y-z translation to obtain maximum signal as outlined earlier. Usually the detection area is within 0.1-1.0 mm from the Y intersection. Experiments were then conducted. Upon completion of the day's experiments, the chip was flushed with water for 10 minutes, 1 M NaOH for 10 minutes and water again for 10 minutes. The device was then stored wet with water until further use.

Analysis of the data was done using Igor Pro software. The data was smoothed using 17 point 2 nd order Savitzky Golay function. Using the statistics function in Igor Pro, the mean and standard deviation of 10 representative seconds of the baseline was determined. The statistics function was also used on the peak to

obtain the maximum. The S/N was calculated by subtracting the mean baseline from the peak maximum and then dividing by the standard deviation of the baseline.

3.3 Results and Discussion

3.3.1 Initial Detection Limit

Initially, before any modifications were made to the system, the detection limit of HRP-Fl was approximately 9.8 μM. This was determined using 2 mg/ml HRP-Fl, 5 mM luminol and 1.5 % H_2O_2 with 10 mM borate pH 10.5 as running buffer. It should be noted that most of the detection limit study was done prior to the pH study presented in Chapter 2, hence the use of pH 10.5 instead of the optimum value. All studies prior to section 3.3.7 were done at pH 10.5, while later data was obtained using the pH 8.5 buffer composition. These experiments were done by performing a 30 s injection of HRP-Fl by applying ground to the sample and inlet buffer reservoirs and -1.2 kV at the sample waste. Separation was achieved by applying -6 kV at the outlet with the post column reservoir floating. The PMT voltage was set at 835 V.

3.3.2 Single-T Injection

The first step taken towards lowering of detection limits involved injecting a larger volume. Originally, the chip was designed to do injections across the double-T, hence, the injection plug size was limited by the geometry of the double-T injector and was independent of time (after a certain minimum time). At that time, the injected volume was approximately 60 pL. This was calculated assuming rectangular channels. Also, the fact that separation buffer was flowing to the

injection waste during injection was taken into account. This accounted for half the volume flowing in the injection waste channel. In order to increase the plug size without major re-designing of the chip, a time dependent injection into the separation channel was done. This was referred to as a single-T injection. The diagram in Figure 3-1 illustrates the double-T and single-T injections.

For these experiments, 180 μg/ml HRP-Fl was used. The running buffer was 10 mM borate at pH 10.5. To combat leakage, hydrodynamic pushback of solution during separation was used. Hence, the normal double-T injection was first carried out, in order to completely refill the sample channel with sample. A 30 s double-T injection at -1.2 kV was conducted. This was followed by a 2 s single-T injection achieved by applying -5 kV at the outlet with A and B still at ground and C at -1.2 kV. Separation was attained by applying ground at B and -6 kV at E with D floating. The PMT was set at 835 V. The new plug size was estimated to be approximately 2 nL. The effect of increasing the injection plug size is illustrated by the electropherograms in Figure 3-2. There was significant bandbroadening with the single-T injection as opposed to the double-T injection. With the double-T injection, 5821 theoretical plates were obtained, whereas with the single-T injection only 964 plates was achieved. However, a detection limit of 0.7 μM was achieved compared to 9.8 μM for the double-T injection.

Subsequently, the single-T injection times and voltages were varied and 1 s at -5 kV was found to be optimum. Under these conditions the injection plug size was calculated to be about 1 nL based on net mobility of the sample, injection time and voltage, plus the double-T volume of about 60 pL. The net mobility was calculated based on the migration time of the sample plug (13 s at -6 kV separation voltage), distance from the injector to the detector and the electric field. The double-T volume was calculated based on the geometry of the double-T injector. A S/N of 14 was

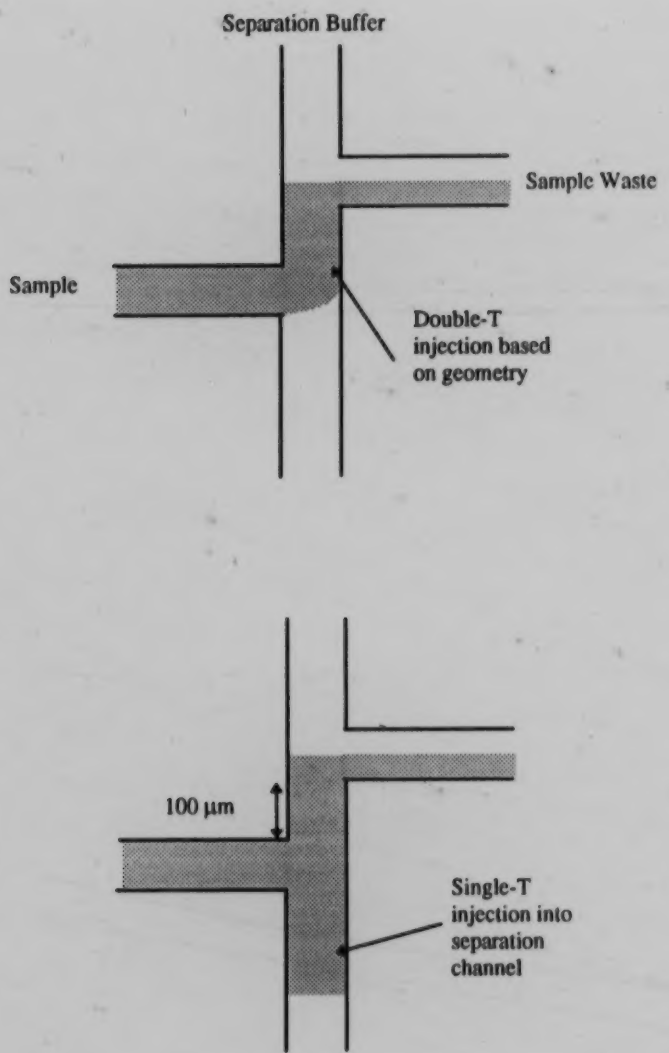

Figure 3-1 Diagram Illustrating Double-T and Single-T injections

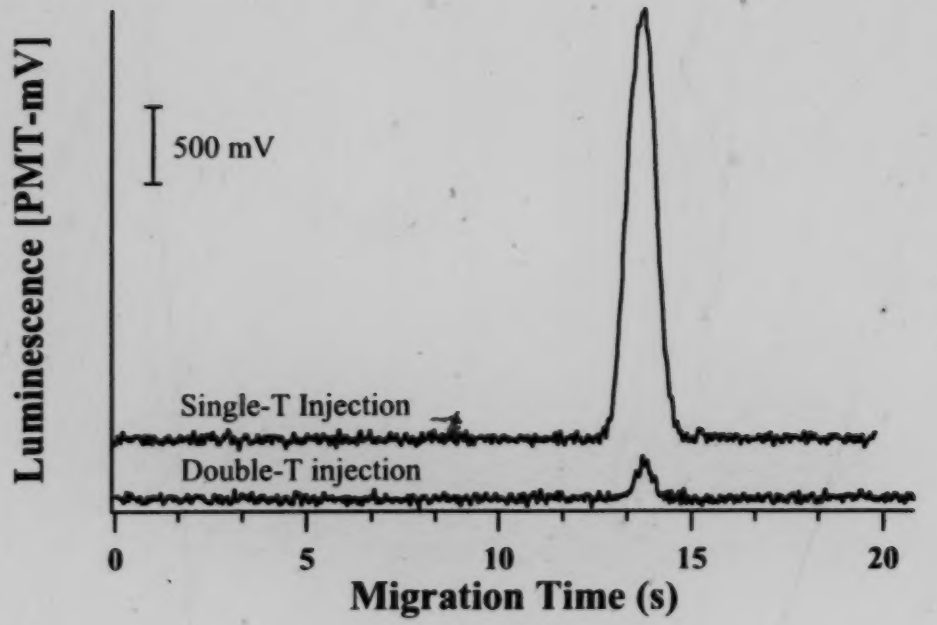

Figure 3-2 Electropherograms Comparing Double-T and Single-T Injections

obtained for 2 mg/ml HRP-Fl using the double-T injection while with the 1s single-T injection a S/N of 138 was obtained. The theoretical plate numbers achieved for these two injections were 5821 for the double-T and 1498 for the single-T injections.

At lower single-T voltages (-3 to -5 kV) longer injection times (2-5 s) were required to produce satisfactory results. However, the resulting peaks were somewhat distorted. Peak distortion seemed to be the result of uneven fluid flow around the T-junction. Fluid flow around the inner corner seemed to be faster than that around the outer corner. Therefore, the sample plug boundary was not at right angles to the channel walls. Hence the resulting peak had a shoulder just before the remainder of the peak eluted. At longer single-T injection times this effect seemed to be exaggerated leading to severe peak distortion. At higher voltages (-5 to -8 kV) and longer single-T injection times (2-5 s), the plug size was so large that extremely broad peaks were produced. Lower injection times were not tried due to difficulties with switching the high voltage relays at a higher speed. The best single-T injection conditions were found to be at a low injection time of 1 s and a high voltage of -5 kV. However, it should be noted that although detection limits were improved by increasing the injection plug size, peak efficiency was decreased quite significantly.

3.3.3 Removal of Optical Filter

In our detection system the light collected by the PMT was filtered through a 450 ± 10 nm band pass filter. The chemiluminescent light emitted in our system was approximately centered at 425 nm. We were using a 450 nm filter since it was the closest one available at the time. The reason the filter was used in the first place was to eliminate background light, since initially the system was not enclosed in a light

tight box. Therefore, to obtain better detection limits the optical filter in the PMT was removed.

A 31 μg/ml HRP-Fl sample was injected for 30 s at -1.2 kV using the double-T injection procedure. This was followed by a 1 s single-T injection at -5 kV. Separation was achieved by applying -6 kV at the outlet and the PMT voltage was set at 835 V. This yielded more signal. Therefore, we were losing quite a bit of light from using a filter which did not match the wavelength of emission. Lower detection limits were achieved and no increase in background was observed. This seems to indicate the light tight box in which our detection system was enclosed was quite efficient at keeping external light out. The detection limit achieved by removing the optical filter was approximately 171 nM with 936 theoretical plates compared to 0.7 μM seen previously. It should be noted that the 0.7 μM detection limit was obtained using a 2 s single-T injection. The electropherograms in Figure 3-3 illustrate the effect of removing the filter on the signal.

3.3.4 Mirror at the Detection Region

In an effort to collect as much light as possible generated by the chemiluminescent reaction we had to find a way of preventing loss of light through the bottom of the device. A mirror was placed below the channels in the detection region. This was done by sputtering aluminum on the back side of the device at the detection area. All the light emitted was reflected upwards to be collected by the objective with no losses through the bottom of the device. Data was collected by injecting 20 μg/ml HRP-Fl across the double-T for 30 s at -1.2 kV followed by a 1 s single-T injection at -5 kV; -6 kV was applied for separation with the PMT set at 835 V. Detection limits were improved by a factor of about 1.6 giving a detection

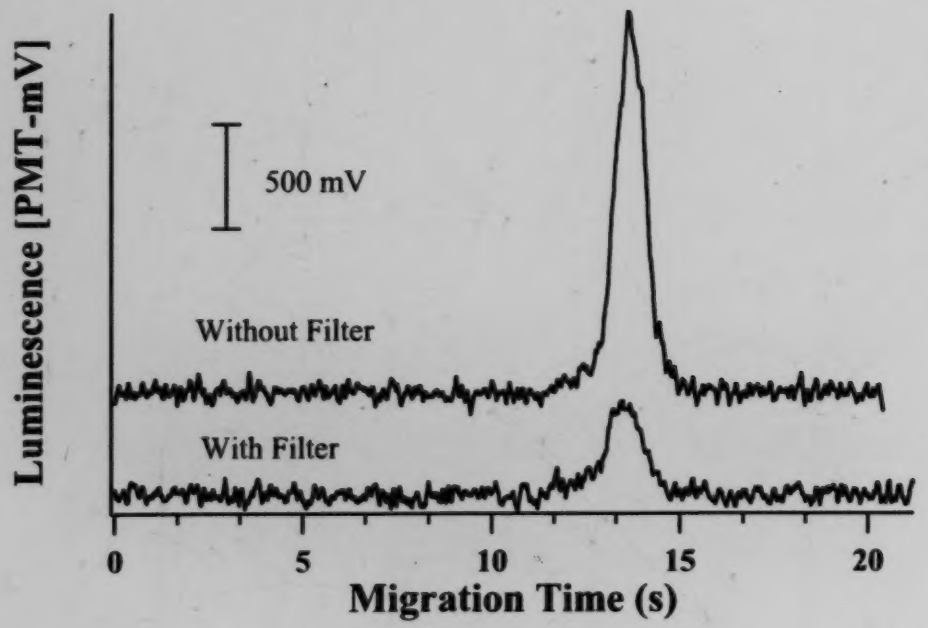

Figure 3-3 Electropherograms Showing Signals Obtained With and Without Filter

limit of about 105 nM and 1186 theoretical plates. A comparison of the signals obtained with and without a mirror present at the detection area is shown in Figure 3-4.

The migration times of the two samples were quite different. This can be accounted for by the use of different microchip devices for separation. The data collected using a mirror at the detection area was done with a new device. The electropherogram "without mirror" was obtained using an "old" device which had been used extensively before and which had undergone several cleaning and conditioning procedures. Hence there may have been significant changes in the ζ potential and hence μ_{eo}, resulting in different migration times. Generally, the trend observed is one where migration time tends to increase with age of the device.

3.3.5 Response to PMT Voltage

Slightly better detection limits were obtained by increasing the PMT voltage. All the previous detection limit experiments were done at 835 V. However, increasing to 900 V resulted in a detection limit of about 88 nM compared to 105 nM obtained at a PMT voltage of 835 V. 1142 plates were obtained at the 900 V PMT setting. It should be noted that as the PMT voltage increased so did the baseline noise. That is, the background noise was amplified. At voltages above 900 V the noise was amplified substantially, so that no significant S/N advantage could be gained. The reagents and conditions used were the same as for the previous experiments done at a PMT voltage of 835 V. The electropherograms in Figure 3-5 compares the signals at the two PMT voltages.

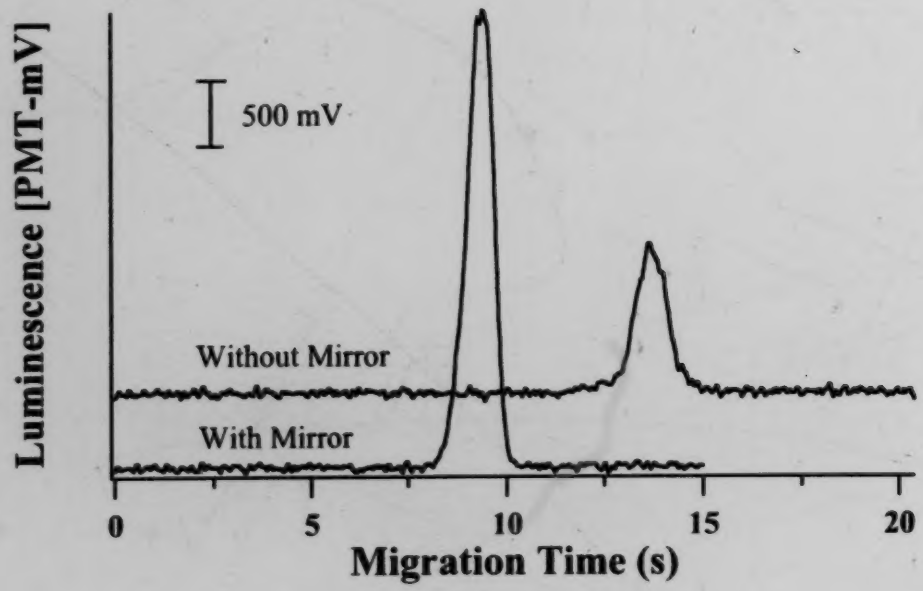

Figure 3-4 Electropherograms Comparing Signals Obtained With and Without Mirror at the Detection Area

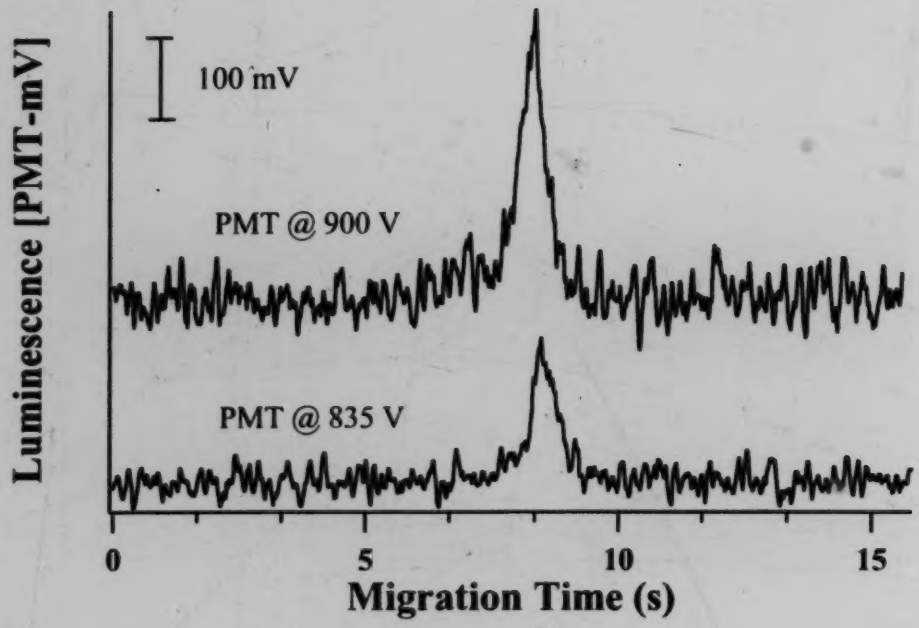

Figure 3-5 Electropherograms Comparing Signals Obtained At Different PMT Voltages

3.3.6 Effect of a Higher N.A. Objective

By using a higher numerical aperture (N.A.) objective the detection limit of HRP-Fl was further lowered to about 56 nM. The instrumental set-up was similar to that previously described, except that a 0.6 N.A. objective was used instead of a 0.35 N.A. objective for light collection. A 20 μg/ml HRP-Fl sample plug was injected across the double-T for 30 s at -1.2 kV followed by a 1 s single-T injection at -5 kV. Separation was effected by applying -6 kV at the outlet with the post column reservoir floating. The device used had a mirror at the detection area and the PMT voltage was set at 900 V. The electropherograms in Figure 3-6 show a comparison of using a 0.35 and a 0.6 N.A. objective for light collection. Here again the migration times are different due to a difference in age of the devices used.

3.3.7 Response to pH

All previous detection limit studies were done at pH 10.5 instead of the optimum at around 8.5 - 9.0. This was because these experiments were done prior to the pH study. The detection limit study was repeated at pH 8.5. The running buffer used was 100 mM borate with 25 mM NaCl and 0.01 % w/v tween 20 at pH 8.5. The reason for all the buffer additives will be discussed later in the next chapter. A 15 μg/ml HRP-Fl sample was injected across the double-T for 30 s at -1.2 kV followed by a 1 s single-T injection at -5 kV. -6 kV was applied for separation. Chemiluminescent emission was collected using the 25X, 0.35 N.A. objective. The PMT voltage was at 900 V and the device had a mirror at the detection area.

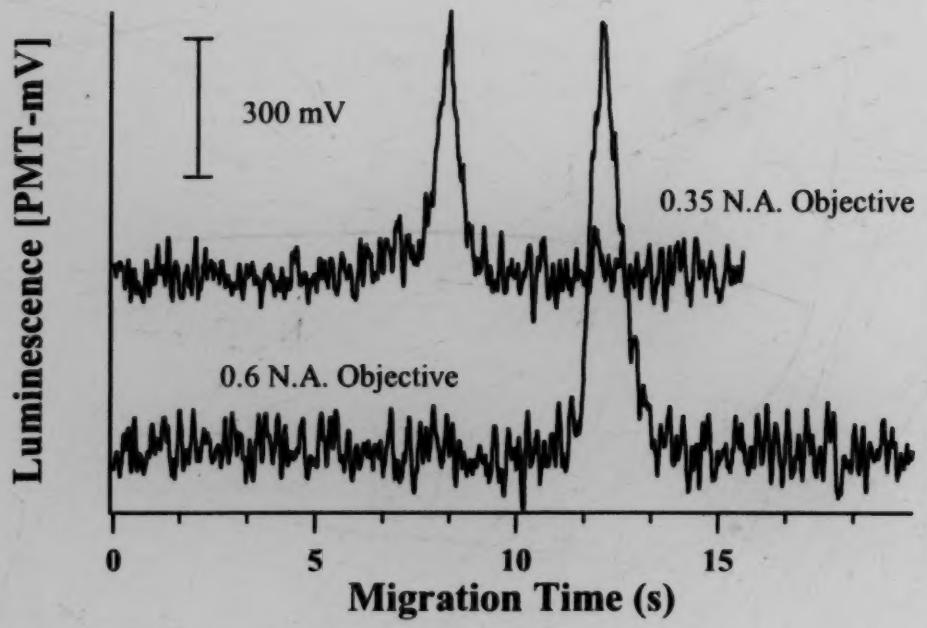

Figure 3-6 Electropherograms Comparing Signals Obtained Using 0.35 and 0.6 N.A. Objectives

Using pH 8.5 a detection limit of 60 nM was achieved, which is higher than the value above, obtained with a 0.6 N.A. lens. However, if this is compared to the previous detection limit of 88 nM obtained using a 0.35 N.A. objective at a PMT voltage of 900 V, there is an improvement using pH 8.5. The electropherograms in Figure 3-7 compares the signal obtained at pH's 10.5 and 8.5 using the 0.35 N.A. objective for light collection. The number of theoretical plates achieved for this detection limit was 1004. The difference in migration times may be due to the differences in pH. However, since these two experiments were carried out in different chips, the age of the device may have been a factor as well.

3.3.8 Effect of Cooled PMT

Experiments done in the summer months reflected a significant increase in the baseline as the temperature of the day increased. An increase of as much as 600 mV could be seen in a single day. To check whether the shifts in baseline affected detection limits, the PMT was cooled using an ice-pack during experiments. These were compared to data obtained without PMT cooling. A 2.7 μg/ml HRP-Fl sample was injected across the double-T for 30 s at -1.2 kV followed by a 1 s single-T injection at -5 kV. Separation was done at -6 kV and the PMT voltage was set at 900 V. A mirror was used at the detection area of the device. The results obtained are displayed by the two electropherograms in Figure 3-8. They show that cooling the PMT does not give a lot more signal. However, the baseline noise is reduced quite a bit. Hence, better detection limits are achieved by cooling the PMT. A detection limit of 35 nM with 1036 theoretical plates was achieved by cooling the PMT compared to the 60 nM obtained previously.

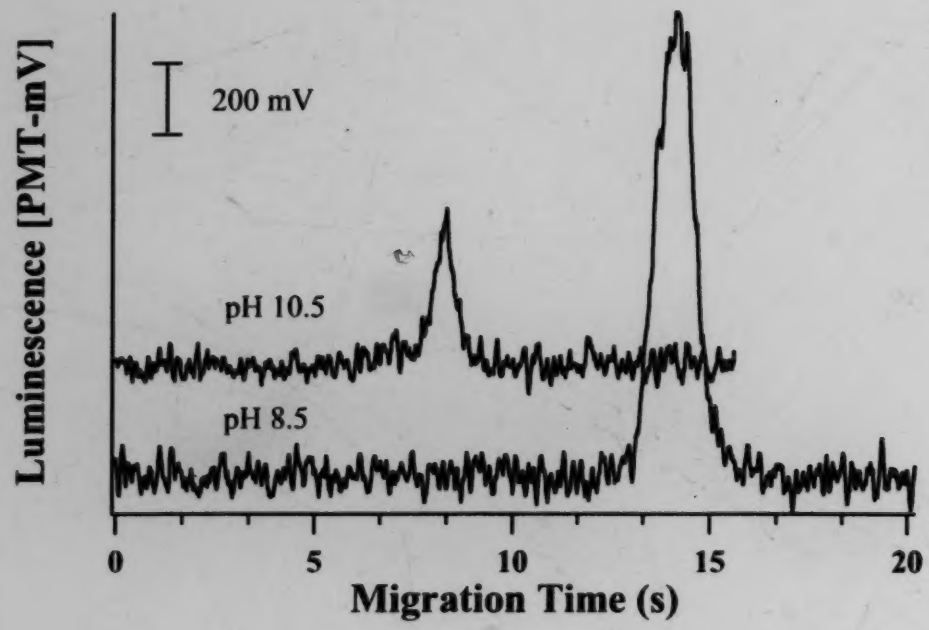

Figure 3-7 Electropherograms Obtained at Different pH's

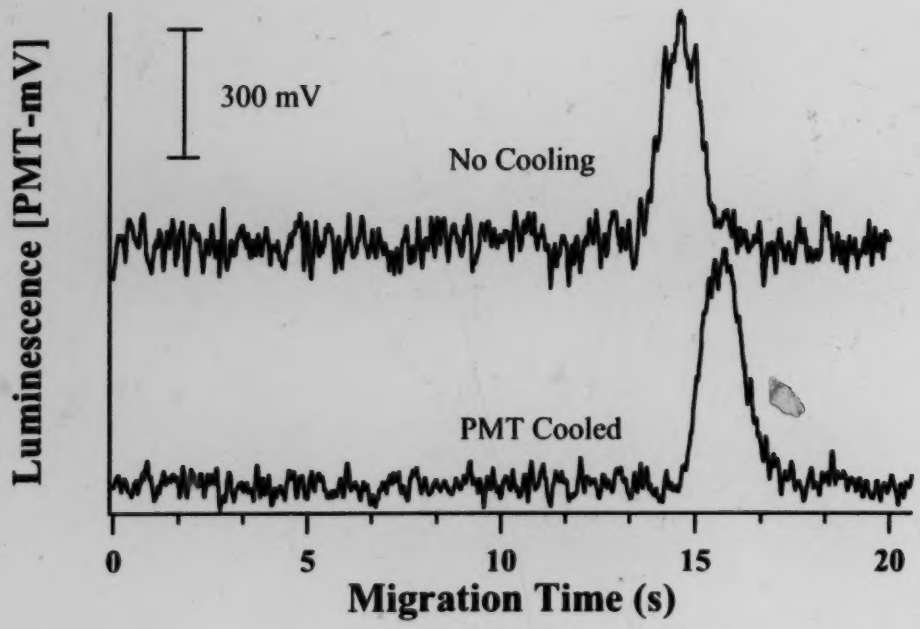

Figure 3-8 Comparison of Signals Obtained With and Without PMT Cooling

3.3.9 Devices with Larger Channels

Better detection limits were obtained by using devices with 40 μm deep channels as opposed to the 10 μm deep channels used in all previous experiments. Using the 40 μm deep devices, 1.6 μg/ml HRP-Fl was injected for 30 s across the double-T injector at -1.2 kV followed by a 1 s single-T injection at -3 kV. This gave an injected volume of about 8 nL. Separation was effected by applying -3 kV at the outlet with the post separation channel floating. The PMT was cooled using an ice-pack and the voltage was set at 900 V. A mirror was used at the detection area. The running buffer consisted of 100 mM boric acid with 25 mM NaCl and 0.01 % w/v tween 20 at pH 8.5. The single-T injection and separation voltages were set at -3 kV instead of -5 kV and -6 kV respectively. This was due to extremely high currents at the higher voltages because of the increase in channel size.

The results were compared to the data obtained in the previous section, which discussed the effect of PMT cooling, where 10 μm deep channels were used. The electropherograms in Figure 3-9 compares data obtained with 10 μm and 40 μm deep channels. A detection limit of approximately 9 nM, which corresponds to approximately 75 attomoles was obtained. However, the peaks separated in the 40 μm deep channels were much broader than those separated in the 10 μm deep devices. Hence, lower efficiencies were obtained. 870 theoretical plates were obtained in the 40 μm device compared to 1036 in the 10 μm device.

Lower efficiencies can be partly accounted for by the lower separation voltage used. At lower separation voltages, migration times are larger, therefore bandbroadening is more severe, resulting in lower plate numbers. However, the peak variance changes by 3×10^{-3} cm^2 for the two devices, while with a diffusion

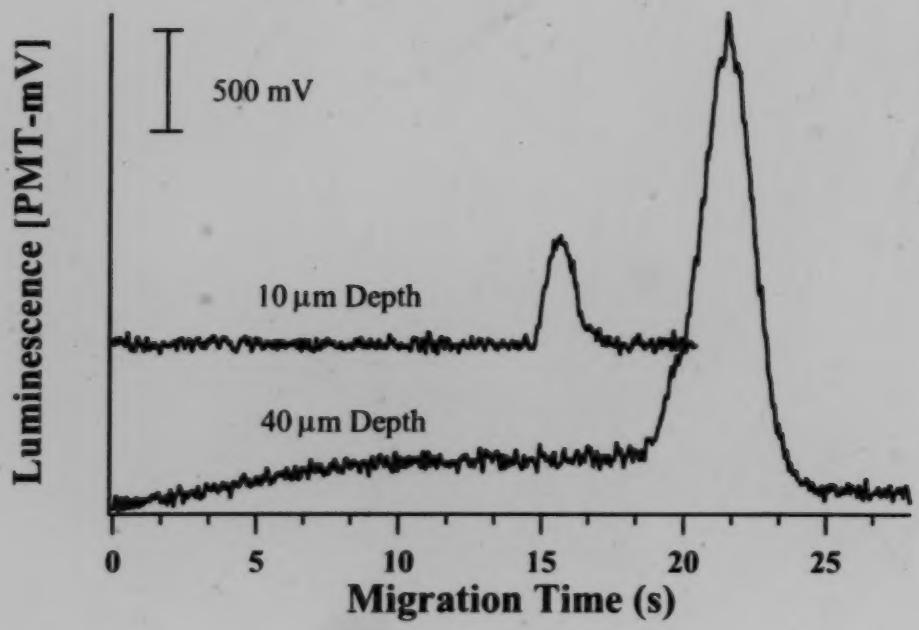

Figure 3-8 Comparison of Devices With Different Sizes of Channels

coefficient of 1 x 10^{-6} assumed the migration time differences gives a variance ($2D\Delta t$) of only 1 x 10^{-5} cm^2. Joule heating may have been responsible for some of the bandbroadening observed. In 10 μm devices, currents typically ranged from 15-20 μA at -6 kV applied voltage. However, with the 40 μm devices, currents exceeded 40 μA at -3 kV applied voltage. Therefore, heating effects will be more severe in the devices with larger channels. The larger channels are more prone to convective mixing of solution due to heating, which contributes to bandbroadening, although the power input to 10 μm devices, at 90 mW, is not that much smaller than the 120 mW in the 40 μm devices. Also, as reported by Fan and Harrison,[10] larger capillary channels on-chips gave lower efficiencies. The effect was not explained, but seemed to be related to leakage from the injector region giving increased bandbroadening.

For this experiment, since the separation voltage is halved, the migration time is expected to double. However, this was not the case. The age difference of the two devices may account for this. The 10 μm deep device was old compared to the 40 μm deep device. The trend observed with devices is that where the migration times increased with age. This is consistent with the results obtained. The migration observed in the old device was not half that seen in the new device, since its age led to longer migration times.

3.4 Conclusions

In this chapter we showed that nanomolar detection limits can be achieved using chemiluminescence detection in microchip based capillary electrophoresis. However, this was at the expense of peak efficiencies. Figure 3-10 summarizes the steps taken to achieve this detection limit. The first bar shows the detection limit before any modifications were made to the system. The second bar shows the

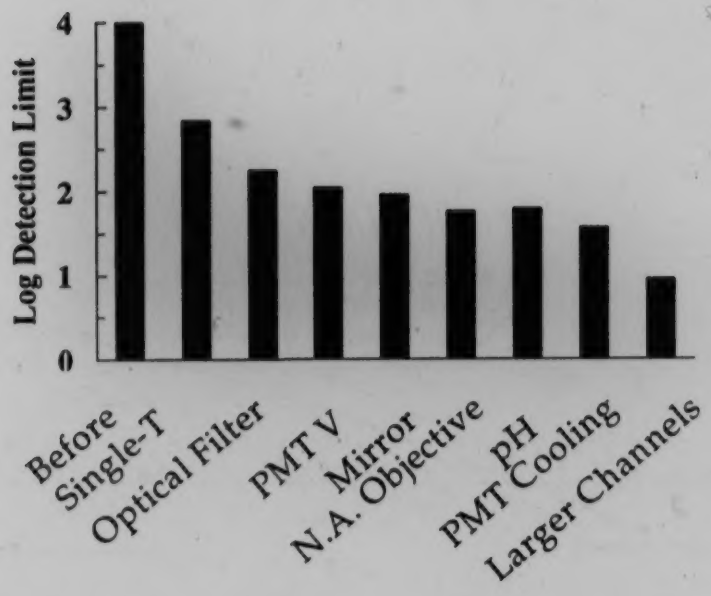

Figure 3-10 Illustration of Detection Limits Achieved After Each Modification to the System

detection limit achieved by increasing the injection plug size using a single-T injection. This was followed by removal of the PMT filter illustrated by the third bar and use of a mirror at the detection area is shown by the fourth bar. The fifth bar shows the effect of increasing the PMT voltage. The sixth bar was obtained by using a higher N.A. objective and the seventh bar by lowering the pH of the system. The eight bar was obtained by cooling the PMT and the ninth bar shows a detection limit of 9 nM achieved by using a 40 μm deep channel as opposed to a 10 μm deep device. Although our detection limit was in the low nanomolar range, by no means is this the best achievable results. The use of enhancers can greatly improve chemiluminescent emission intensity resulting in lower detection limits.

For the horseradish peroxidase catalyzed reaction of luminol and hydrogen peroxide, there is a wide variety of compounds that can be used to increase light output. The degree of enhancement can be several hundredfold or thousandfold depending on the species used. One of the best enhancers of luminol/HRP/H_2O_2 is p-iodophenol which yields an enhancement of 2500 with luminol.[11] Other enhancers include phenol, p-hydroxybenzoic acid, p-hydroxymethylbenzoate, p-hydroxybenzaldehyde, and aniline which yield an enhancement of 2-40 times.[12] Sun, Kricka and Dunford reported that 4-substituted arylboronic acids increase the light emission by >10-fold. They also claimed that 4-biphenylboronic acid yield greater enhancement than p-iodophenol.[13] However, this is in contradiction with the Encyclopedia of Anal Sci[11] which report that p-iodophenol yields an enhancement of 2500. The real value in our system probably has to be determined experimentally. However, it is certainly worth trying in the future.

It has also been reported that chemical indicators may be used as enhancers in the luminol/HRP/H_2O_2 reaction. Indicators such as phenol red, phenolphthalein, cresol red, cresolphthalein, o-toludine and benzidine were used. Enhancements of

2-80 times have been observed. The authors reported that phenol derivatives gave maximum emission at pH 8.5, while emission was maximum at pH 10.5 for aniline derivatives. In addition, a methyl group ortho or para to the OH and NH_2 groups in the benzene ring showed an inhibitory effect at high concentrations.[14] Use of phenol derivatives should prove to be quite useful for enhancement in our system since it is necessary for us to work at lower pH.

It should be noted that these enhancers were used in systems where the signal was integrated over time, unlike our system where the signal is measured as the sample flows past the detector. Hence, the magnitude of enhancement reported by those authors may not be as great with our system, but it is still worth trying. By no means is this list exhaustive of all the possible enhancers. However, when choosing an enhancer, several factors should be considered. Among them are the compound's compatibility with our reaction system. Factors such as pH, concentration, buffer conditions, cross reactions and stability are some of the things that need to be considered. To further improve detection limits, entire new chemiluminescent systems may be tried.

Luminol belongs to a class of compounds called acylhydrazides. In luminol chemiluminescence, the quantum yield of luminol is about 1.0-1.5 % in aqueous systems. Use of more efficient systems can result in better detection limits. The catalysts and oxidizing agents used with luminol may be used with its derivatives to produce chemiluminescence. Aminobutylethyl-napthalhydrazide has a quantum yield which is about four times that of luminol. However, this compound is easily oxidized at the surface of the solution by oxygen in the air. The most efficient chemiluminescent hydrazide discovered is a benzoperylene derivative with a quantum yield of 700-800 % compared to luminol.[15] Other chemiluminescent systems which are not based on acylhydrazides may be tried as well, however, attention should be

paid to the conditions required to ensure their compatibility with microchip capillary electrophoresis. Special attention should be paid to pH.

In conclusion, chemiluminescence detection in microchip capillary electrophoresis has proven to be quite capable of detecting low levels of analyte. It is far better than UV detection but not as good as fluorescence detection. However, there is still room for improvement with a bright, promising future for chemiluminescence detection in microchip capillary electrophoresis.

3.5 References

(1) Dadoo, R.; Colon, L. A.; Zare, R. N. *J. High Resolut. Chromatogr.* **1992,** *15*, 133-135.

(2) Baeyens, W. R. G.; Ling, B. L.; Imai, K.; Calokerinos, A. C.; Schulman, S. G. *J. Microcolumn Sep.* **1994,** *6*, 195-206.

(3) Campana, A. M. G.; Baeyens, W. R. G.; Zhao, Y. N. *Anal. Chem.* **1997,** *69*, A83-A88.

(4) Hara, T.; Nishida, H.; Nakajima, R. *Anal. Sci.* **1994,** *10*, 823-825.

(5) Zhao, J. Y.; Labbe, J.; Dovichi, N. J. *J. Microcolumn Sep.* **1993,** *5*, 331-339.

(6) Huang, B.; Li, J. J.; Zhang, L.; Cheng, J. K. *Anal. Chem.* **1996,** *68*, 2366-2369.

(7) Hara, T.; Nishida, H.; Kayama, S.; Nakajima, R. *Bull. Chem. Soc. Jpn., Apr* **1994,** *67*, 1193-1195.

(8) Hara, T.; Kayama, S.; Nishida, H.; Nakajima, R. *Anal. Sci.* **1994,** *10*, 223-225.

(9) Hara, T.; Yokogi, J.; Okamura, S.; Kato, S.; Nakajima, R. *J. Chromatogr. A* **1993,** *652*, 361-367.

(10) Harrison, D. J.; Fan, Z. H. *Anal. Chem.* **1994,** *66*, 177-184.

(11) Nieman, T. A. In *Encyclopedia of Analytical Science*; Townshend, A., Ed.; Academic Press, 1995; Vol. 1, pp 608-621.

(12) Sanchez, F. G.; Diaz, A. N.; Garcia, J. A. G. *Journal Of Luminescence* **1995,** *65*, 33-39.

(13) Sun, W.; Ji, X.; Kricka, L. J.; Dunford, H. B. *Can. J. Chem.* **1994,** *72*, 2159-2162.

(14) Diaz, A. N.; Sanchez, F. G.; Garcia, J. A. G. *Journal Of Photochemistry And Photobiology A Chemistry* **1995,** *87*, 99-103.

(15) Rongen, H. A. H.; Hoetelmans, R. M. W.; Bult, A.; Van Bennekom, W. P. *J. Pharm. Biomed. Anal.* **1994,** *12*, 433-462.

CHAPTER 4

CHEMILUMINESCENT IMMUNOASSAYS IN MICROCHIP CAPILLARY ELECTROPHORESIS

4.1 Introduction

Chemiluminescence is very sensitive but lacks selectivity.[1-4] Immunoassays are both specific and sensitive.[5, 6] Capillary electrophoresis is a powerful separation technique because of its capabilities of analyzing complex mixtures with high resolution in relatively short analysis times, utilizing picoliter to nanoliter sample volumes.[1, 3, 4] Hence, combining immunoassays with chemiluminescence detection in capillary electrophoresis promises to be quite useful in the real world. In this chapter, application of chemiluminescence detection in microchip capillary electrophoresis to immunoassays is demonstrated.

For a number of years radioimmunoassays were quite popular. However, due to the instability of radiolabelled reagents, the health hazard posed by radioactive labels and problems with waste disposal,[5, 7-9] alternative methods are being sought. Chemiluminescence seemed to be a good alternative with several advantages. Since with chemiluminescence there is no need for sample radiation, problems with light scattering, unselective excitation and source instability are eliminated.[10] Low background signal result in good detection limits. Chemiluminescence has a large linear dynamic range which may be up to six orders of magnitude. "Since it is an emission process, the response is usually linearly proportional to the concentration,

from the minimum detectable concentration up to the point where it is no longer possible to maintain excess of reactants relative to the analyte."[2] In addition, most chemiluminescent assays are fast, the reagents are stable and have no known toxic effects.

In our experiments we seek to prepare a calibration curve for the direct, noncompetitive immunoassay reaction of $F(ab')_2$ fragment goat anti-mouse IgG, HRP conjugate and mouse IgG, whole molecule. By adding specific amounts of antigen to a fixed concentration of labeled antibody which is in excess, we expect almost complete reaction of the antigen to form a complex with the antibody. The following equation describes the expected reaction.

$$\mathbf{Ab^*\ (excess) + Ag \rightarrow Ab^*\text{-}Ag + Ab^*\ (free)}$$

Separation of the above reaction products is expected to yield two peaks; one for the complex and the other for the unreacted (free) antibody. As the amount of antigen added increases at a fixed antibody concentration, the peak area of the complex is expected to increase while the free antibody peak area decreases. We anticipate that at some point in time, both the Ab*-Ag and Ab* curves will begin to level off, indicating that most of the Ab* has been consumed. At low antigen concentration the calibration curve for both complex and free antibody is expected to be linear, with a negative slope for Ab* and a positive slope for Ab*-Ag.

In our system, the reaction is homogeneous. i.e. it is done in a single phase. However, by convention, immunoassay reactions which involve separation of free and complexed fractions are termed heterogeneous assays. Therefore, from a chemistry point of view, our reaction is homogeneous. However, from an immunoassay perspective, our system is heterogeneous.

In this chapter we will show that at low mouse IgG concentrations, the anti-mouse IgG/mouse IgG reaction is linear. We will also show that at higher mouse IgG concentrations the curve begins to level off indicating that a saturation point is being reached.

4.2 Experimental

4.2.1 Device Fabrication and Instrumentation

Devices were fabricated in Pyrex glass using the procedures described in Chapter 2. All devices used were 10 μm deep and had aluminum mirrors on the back side at the detection area. The instrumental set-up was similar to that presented in Chapter 2. All experiments were conducted by injecting a plug of sample across the double-T injector for 30 s by applying ground potential at the sample and buffer reservoirs and -1.2 kV at the sample waste reservoir. This was immediately followed by a 1 s single-T injection done by applying -5 kV at the outlet. Separation was achieved by applying ground at the separation buffer and -6 kV at the buffer waste with the post-column reservoir floating. Chemiluminescent emission was collected by a 25X, 0.35 N.A. objective positioned above the device 0.1-1.0 mm after the Y intersection and directed into a PMT. The PMT was cooled using an ice pack and the voltage was set at 900 V. No optical filter was used in the PMT. The signal was amplified using a 10^8 Ω impedance amplifier and routed through a 25 Hz noise filter before being recorded both on a chart recorder and a Macintosh computer. The A/D board sampling rate was 100 Hz.

4.2.2 Materials

In all experiments 100 mM borate buffer containing 25 mM NaCl (BDH, Toronto, ON) and 0.01 % w/v tween 20 (Sigma, St. Louis, MO) at pH 8.5 was used. This was prepared by dissolving the required amounts of boric acid (J. T. Baker, Phillipsburg, NJ) and buffer additives in Millipore water and adjusting to pH 8.5 using 1 M NaOH (BDH). 5 mM luminol (Sigma) and 1.5 % H_2O_2 (Caledon, Georgetown, ON) prepared in running buffer was used in all experiments. H_2O_2 was prepared fresh each day by diluting the 30 % reagent to the required concentration. Samples consisted of various mixtures of $F(ab')_2$ fragment goat anti-mouse IgG, HRP conjugate (Pierce, Rockford, IL) and mouse IgG, whole molecule (Pierce). In some cases microperoxidase (Sigma) was added to the sample as an internal standard. 5 μM stock solution of microperoxidase was prepared by dissolving the required amount of enzyme in buffer.

The anti-mouse IgG came as a lyophilized powder which was restored by dissolving in Millipore water as suggested by the supplier. However, the storage procedures used were different from that recommended. According to Pierce, the restored product is stable for several weeks if stored at 4 °C. Also, the shelf life may be extended to one year by adding an equal volume of glycerol (50 % final concentration) and storing at -20 °C. Unfortunately, the stability of the sample after restoration and storage at 4 °C was not so good, and we had trouble working with glycerol present in the sample as it resulted in unusual flow behaviour and blockages in the chips. We therefore resorted to our own storage method which was to divide the solution immediately after restoration into single use aliquots and storing them at -20 °C without glycerol. We were able to use these samples for up to a month without any problems. The samples may be stable for longer under these conditions but we did not try using the solutions beyond one month.

Mouse IgG was stored at 4 °C as specified by the supplier without any difficulty. Luminol was stored at room temperature away from light. Hydrogen peroxide reagent was stored at 4 °C. Microperoxidase stock solution was stored at 4 °C protected from light.

Samples were prepared just before use by adding the required amounts of mouse IgG and microperoxidase (if used) to the aliquoted portion of anti-mouse IgG and diluting to volume with filtered buffer. The sample was vortexed for approximately 5 seconds and incubated in the dark at room temperature for at least 15 minutes prior to use. No further filtration of the sample was done. All other solutions used on-chip were filtered. Luminol and H_2O_2 were filtered through 0.22 μm cellulose acetate syringe filters (Millipore, Bedford, MA) and buffers were filtered using 0.22 μm nylon syringe filters (Micron Separations Inc., Westboro, MA).

Each day before the start of experiments the chip was flushed and flows were checked as described previously. This was followed by the optimization process. Upon completion of experiments the chip was cleaned again as outlined in Chapter 2 and stored filled with water until further use.

To demonstrate that there is a linear relation of the immunoassay reaction at low Ag concentrations, samples containing 0, 10, 20, 30, 40, 50 and 60 μg/ml of mouse IgG with a fixed 53 μg/ml anti-mouse IgG were injected and separated. To show a saturation point is reached in this immunoassay reaction, samples containing 0, 44, 88 and 176 μg/ml of Ag added to 53 μg/ml Ab* were injected and separated. For samples containing internal standard, 0, 10, 20, 30, 40 and 50 μg/ml Ag solutions containing 53 μg/ml Ab* and 0.3 μM microperoxidase were injected and separated.

4.3 Results and Discussion

4.3.1 Preliminary Immunoassay Reaction

Prior to using 100 mM borate buffer with 25 mM NaCl and 0.01 % tween 20 at pH 8.5, 10 mM borate buffer at pH 8.5 was used. The first studies were done without internal standard. The sample containing no Ag was injected and separated first and a single peak was obtained as expected. Injecting all other samples containing Ag also gave single peaks, which decreased with increasing Ag concentration. This was surprising as two peaks were expected; one for Ab*- Ag complex and the other for free Ab*. The electropherograms in Figure 4-1 illustrate the decrease observed with increasing Ag concentration.

Based on migration time and peak size, the single peak obtained seemed to be that of the free Ab* and not for the complex. Initially we thought that the complex zone was co-migrating with the free Ab* zone, or that the complex was being adsorbed onto the channel walls. To combat these problems we reduced the EOF by increasing the ionic strength of the buffer system and added a surfactant to prevent adsorption with the hope of achieving separation of the Ab*-Ag and free Ab*. Previous experience with adding these agents in ours and other labs, indicated adsorption would be reduced.[11, 12]

The ionic strength was increased by increasing the concentration of boric acid from 10 mM to 100 mM and by the addition of 25 mM NaCl. For reducing adsorption, we chose a neutral surfactant, tween 20. We used 0.01 % w/v tween 20 in our buffers. Unfortunately, none of this enabled us to obtain a peak for the complex. So, we suspected that some other factors may be responsible for this behaviour. Apart from the possibility of adsorption being extremely severe, we thought that the

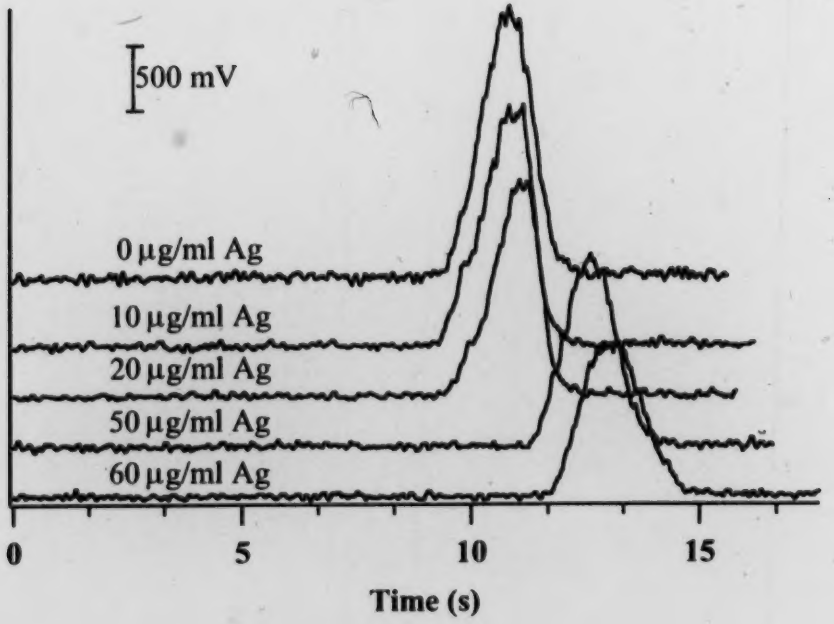

Figure 4-1 Electropherograms Showing the Decrease in Ab* as Ag Increased

complex may be precipitating, or it may be migrating in the opposite direction (towards the inlet). Therefore, we resorted to measuring the reaction of Ab* and Ag based on the decrease in peak areas of the free Ab*, instead of an increase in complex. We continued using 100 mM borate buffer with 25 mM NaCl and 0.01 % w/v tween 20 at pH 8.5.

4.3.2 Calibration Curve Without Internal Standard

Using no internal standard, a calibration curve was constructed for the immunoreaction of $F(ab')_2$ fragment goat anti-mouse IgG, HRP conjugate and mouse IgG, whole molecule. The curve, obtained by injecting samples containing 0, 10, 20, 30, 40, 50 and 60 μg/ml of mouse IgG with a fixed 53 μg/ml anti-mouse IgG, is illustrated in Figure 4-2. The plot shows peak area versus antigen concentration.

During experiments, gel-like precipitates formed in the sample channels across the double-T injector all the way to the sample waste channels. The formation of these precipitates were especially predominant when increasing amounts of Ag concentrations were used. Also, there were noticeable increases (1-2 %) in migration time between runs, and the background signal increased significantly as Ag concentration in samples increased. Sometimes there were traces of this material in the separation channel as well. This led us to believe that the Ab*-Ag complex was not being adsorbed onto the channel walls, but instead, it was precipitating out of solution. The precipitates were severe enough to cause blockages, if they were not cleaned at an early stage. This forced us to clean and equilibrate the chip again before completing a set of experiments for the calibration curve.

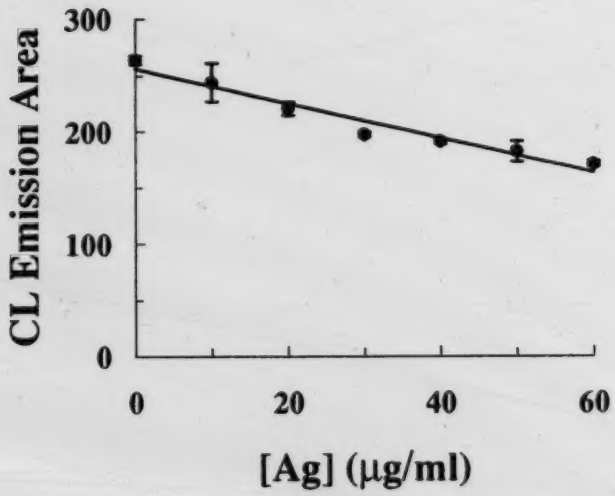

Figure 4-2 Ab*-Ag Calibration Curve Without Internal Standard

We have had previous experiences where electroosmotic flow (EOF) changes after NaOH rinses. This may be observed by the migration time change for Sample A and Sample A2 shown in Tables 4-1 and 4-2. Sample A2 is really sample A which was injected and separated a second time after cleaning the chip. A 6-8 % change in migration time was observed. Meanwhile, during consecutive injections and between sample changes, the elestroosmotic flow was also changing. For consecutive injections of a given sample, the migration times were changing by 1-2 %. However, EOF shifts were more obvious between sample changes, with the largest changes occurring with samples at higher antigen concentrations. Migration time shifts of up to 4 % were observed. Hence, from the start of the calibration curve to the end, a total of about 15-20 % shift in migration time was often observed.

This behavior may be accounted for by the precipitation of Ab*-Ag complex. Build-up of precipitate from previous samples may be a contributing factor as well. Precipitation causes the resistance in the channels to increase resulting in decreased flow. Hence migration times increase. This is in accordance with the trend observed, where the migration times increased with increasing Ab*-Ag. As the Ab*-Ag complex, and hence the amount of precipitate, increased, so did the resistance. Therefore, the flow decreased and the migration times increased.

In capillary electrophoresis, peak area varies inversely with solute velocity. Since solute velocity is directly related to EOF, ($v = \mu_{eo}V/L$) we had to correct for flow changes. According to W. J. Lambert and D. L. Middleton,[13] "... a small change in electroosmotic flow may have dramatic effects on the peak area. This change may occur under constant field strength due to hysteresis." In this article, to correct for flow changes it was suggested that the peak areas be normalized by multiplying by the inverse migration time. Therefore, in the treatment of our data, we normalized the peak areas by dividing by their respective migration times.

To combat the problem of chip fouling, the chip was recleaned and conditioned using the standard procedure followed at the beginning of the day after every 3-4 samples depending on how quickly the results degraded. In order to account for changes and to make the results comparable to those obtained before recleaning, the sample containing no Ag was used as a blank and injected and separated again. The results obtained for these second set of experiments were normalized to those obtained previously; all subsequent data were standardized using this correction factor until another cleaning was required. The following equation describes all corrections made to the data.

$$\frac{\textbf{Avg (Pk Area/}t_m\textbf{) for first Blank (A)}}{\textbf{Avg (Pk Area/}t_m\textbf{) for Blank after cleaning (A2)}} = \textbf{Correction Factor}$$

The data obtained, and its treatment, is displayed in Table 4-1. Using the correction procedure described above a linear fit to the data was obtained, with a slope of -1.5472, an intercept of 256.1685 and an R^2 value of 0.9548. The standard errors in the slope and intercept are 0.1505 and 5.4263 respectively. The standard error of the y-estimate was calculated to be 7.9636. The results are shown in Figure 4-2. Each data point represents the average of five injections whose peak areas were corrected for changes in migration times and chip cleaning between samples, if applicable. The error bars indicate the standard deviation.

4.3.3 Calibration curve Using an Internal Standard

Since no peaks were obtained for the Ab*- Ag complex, and the extent of Ab* reaction was being based on the decrease of free Ab*, we added an internal standard to the samples to account for injection variations. We had three available enzymes as

Sample/[Ag]	t(mig)	Peak Area	Pk Ar/t(mig)	Corr Pk Ar	Avg Pk Ar	Std Dev
A	10.6571	2763.97	259.3547963		263.79323	3.8006607
0 µg/ml	10.693	2816.39	263.3863275			
	10.7369	2838.51	264.3696039			
	10.7745	2905.89	269.7006822			
	10.8254	2837.93	262.1547472			
B	10.7525	2702.5	251.3368984		243.7289	17.14784
10 µg/ml	10.7793	2832.92	262.8111287			
	10.7884	2593.63	240.4091432			
	10.8113	2674.44	247.3745063			
	10.8366	2348.43	216.7128066			
C	10.9415	2450.2	223.936389		220.23454	5.9957467
20 µg/ml	10.9613	2502.14	228.2703694			
	10.9587	2364.77	215.7892816			
	10.9718	2410.33	219.6840992			
	10.9868	2345.6	213.4925547			
A2	11.3407	2620.11	231.0360031			
0 µg/ml	11.3286	2661.4	234.9275286			
	11.2973	2866.17	253.7039824			
	11.2977	2867.1	253.7773175			
	11.3107	2915.17	257.7355955			
D	11.732	2181.58	185.9512445	199.209955	197.31335	2.3861317
30 µg/ml	11.7802	2169.33	184.1505238	197.280839		
	11.8382	2207.35	186.4599348	199.754916		
	11.8813	2180.01	183.4824472	196.565127		
	11.9458	2160.52	180.8602187	193.755928		
E	12.3477	2249.11	182.1480924	195.13563	190.9907	2.5052723
40 µg/ml	12.4014	2194.69	176.9711484	189.589559		
	12.4277	2218.88	178.5430933	191.273587		
	12.459	2212.96	177.6193916	190.284024		
	12.5087	2202.95	176.1134251	188.670679		
F	12.5213	1988.34	158.7966106	170.119139	181.76222	9.1235452
50 µg/ml	12.5631	2072.63	164.9775931	176.740839		
	12.5931	2116.27	168.0499639	180.032276		
	12.6317	2250.72	178.1802924	190.884918		
	12.6334	2252.78	178.3193756	191.033918		
G	13.0699	2047.19	156.6339452	167.802271	170.44878	2.6308846
60 µg/ml	13.0959	2060.95	157.3736818	168.594753		
	13.1386	2132.94	162.3414976	173.916784		
	13.1668	2120.05	161.0148252	172.495517		
	13.2122	2089.61	158.1576119	169.434579		

Table 4-1 Showing Treatment of Data Obtained Without Internal Standard

possible candidates for internal standards: HRP, HRP-Fl and microperoxidase. These were all tried, but only microperoxidase was resolved from the Ab* peak. HRP and HRP-Fl co-migrated with the Ab*. Therefore, we used microperoxidase as internal standard. This was done by adding enough stock 5 μM microperoxidase solution to the sample to give a final concentration of 0.3 μM. Injection and separation produced two peaks; one for MP and the other for Ab*. The electropherogram in Figure 4-3 illustrates the separation of antibody and microperoxidase.

In treating this data, first the peak areas for both free Ab* and MP were corrected by dividing by their respective migration times, as described in the previous section. Then the ratio of Ab*/MP was calculated for each run. For experiments done after recleaning, the blank sample was also repeated. The results were corrected for flows and the ratio of Ab*/MP standardized against the first Ab*/MP ratio obtained for the blank. This was done by dividing the first blank Ab*/MP ratio by the Ab*/MP obtained after cleaning the chip. This gave a correction factor for all subsequent Ab*/MP ratios obtained after recleaning. Finally, all the Ab*/MP ratios were multiplied by the average MP peak area obtained for the first blank. The following equations describe the corrections made to the data.

Calculation of Ab*: MP ratio:

$$\frac{\textbf{Ab* Pk Area}/t_m}{\textbf{MP Pk Area}/t_m} = \textbf{Ab*: MP Ratio}$$

Calculation of correction factor for data obtained after chip cleaning:

$$\frac{\textbf{Avg (Ab*: MP) for first Blank (A)}}{\textbf{Avg (Ab*: MP) for Blank after cleaning (A2)}} = \textbf{Correction Factor}$$

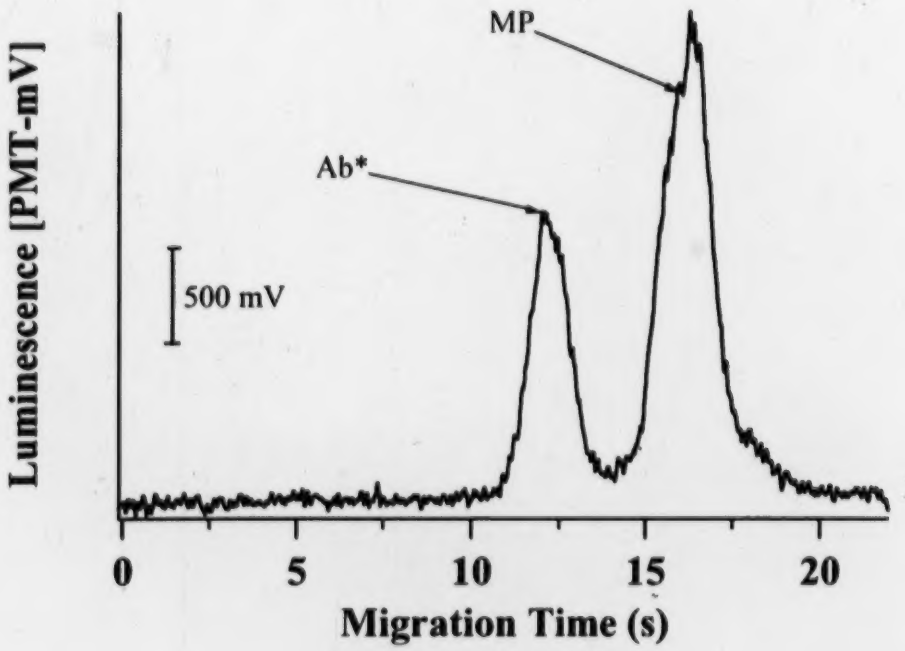

Figure 4-3 Electropherogram Showing the Anitbody with Microperoxidase

This correction factor was used to correct the average Ab*: MP ratio for data obtained after cleaning. Figure 4-4 illustrates a plot of corrected Ab*: MP ratios versus Ag concentration. Each data point represents the average of five corrected Ab*: MP peak area ratios, and the error bars reflect the standard deviations. To obtain the corrected peak areas, the corrected Ab*: MP ratios were multiplied by the average MP peak area obtained for the first blank. While this calculation is not normally done when using an internal standard, its use allowed a comparison of the slopes with and without the internal standard present.

Correction Factor x Avg Ab*: MP x Avg (MP Pk Area/t_m) = Corr. Pk Area

Since an internal standard was used, there should be no need for a correction factor. However, from the data obtained, the ratios of the blank samples run before and after cleaning were significantly different. A Q-test was done at 90 % confidence level in order to reject bad data points in the data set for samples A and A2. Then a T-test was carried out at a 95 % confidence level to determine whether the means of A and A2 were statistically different. The analysis revealed that the means were indeed different. Therefore, we used a correction factor to normalize the data sets obtained after cleaning the chip to those obtained before cleaning.

Table 4-2 and 4-3 illustrate the raw data and its treatment to obtain the final values. A plot of corrected Ab* peak areas versus Ag concentration is presented in Figure 4-5. A linear fit of the data was obtained, with an R^2 value of 0.9867, an intercept of 174.0694 and a slope of -1.2999. The standard errors of the intercept and slope were 2.2830 and 0.0754, respectively. The standard error of the y-estimate was found to be 3.1545. Compared to the data set obtained without internal standard, the trends are similar. It was noted that the absolute emission intensities of the Ab* in the presence of MP was less than that obtained without MP. However, the slopes of the

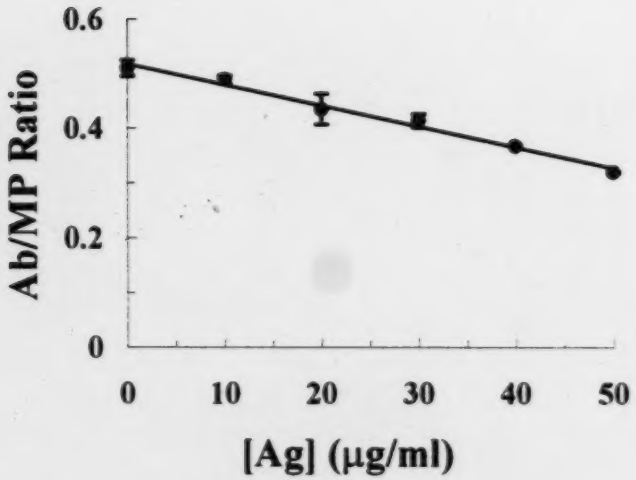

Figure 4-4 Ab*/MP Ratio versus [Ag]

Sample/[Ag]	t(mig) 1	t(mig) 2	Area 1	Area 2	Ar 1/t(m) 1	Ar 2/t(m) 2	Ratio
A (Blank)	12.2664	16.2717	2089.07	5331.59	170.30832	327.66029	0.519771
0 μg/ml	12.2678	16.2828	2217.13	5563.93	180.7276	341.70597	0.528898
	12.2371	16.2206	2018.27	5388.24	164.93042	332.185	0.4965017
	12.2091	16.2019	2075.28	5571.95	169.97813	343.9072	0.4942558
	12.2108	16.2025	2088.91	5417.1	171.07069	334.33729	0.511671
Sample B							
10 μg/ml	11.8691	15.549	2348.6	6249.39	197.87515	401.91588	0.4923298
	11.8571	15.5405	2424.05	6428.99	204.43869	413.69261	0.4941802
	11.8374	15.5041	2381.47	6373.54	201.18185	411.08739	0.4893895
	11.8263	15.5232	2410.96	6655.85	203.86427	428.76791	0.4754653
	11.871	15.571	2506.08	6677.89	211.10943	428.86712	0.492249
Sample C							
20 μg/ml	12.2705	16.0668	1543.64	4375.41	125.8009	272.32616	0.4619494
	12.2295	16.0738	1645.48	5442.27	134.55006	338.58017	0.397395
	12.2337	16.0655	2076.84	5922.5	169.76385	368.6471	0.460505
	12.2055	16.0036	1655.29	4984.43	135.61837	311.4568	0.4354324
	12.2165	16.0303	1687.34	5339.08	138.11976	333.06176	0.4146971
Sample D							
30 μg/ml	12.2919	16.1446	1562.29	4975.69	127.09915	308.19531	0.4123981
	12.3108	16.166	1750.09	5645.89	142.15892	349.24471	0.4070467
	12.2879	16.1704	1747.91	5306.26	142.24644	328.14649	0.4334846
	12.2413	16.0782	1258.49	4088.49	102.80689	254.28779	0.4042935
	12.2373	16.1099	1646.3	5348.18	134.53131	331.98096	0.405238
Sample A 2							
(Blank)	13.1271	17.8099	2706.91	4997.37	206.20777	280.59506	0.7348945
0 μg/ml	13.1577	17.8853	2489.61	6024.15	189.21316	336.8213	0.5617613
	13.1745	17.9094	2507.74	6528.16	190.34802	364.51026	0.5222021
	13.2095	17.955	2461.86	5866.48	186.37042	326.73239	0.5704069
	13.2359	18.0108	2442.37	6051.11	184.52618	335.9712	0.5492321
Sample E							
40 μg/ml	13.6309	18.5806	1918.12	6252.76	140.71851	336.52089	0.4181569
	13.6533	18.6327	2068.29	6582.47	151.48645	353.27516	0.4288059
	13.6122	18.5246	2118.39	6773.27	155.62437	365.6365	0.4256259
	13.6235	18.5252	2114.98	6709.03	155.24498	362.15695	0.4286677
	13.6556	18.5724	2183.01	7398.51	159.86189	398.36047	0.4012996
Sample F							
50 μg/ml	13.8026	18.9189	2055.58	7681.06	148.92701	405.99929	0.3668159
	13.8449	19.0248	2250.47	8276.3	162.54866	435.02691	0.373652
	13.8453	19.1315	1959.84	7864.98	141.55273	411.10106	0.3443259
	13.8633	19.2028	1942.75	7183.38	140.13619	374.07982	0.3746157
	13.8887	19.3029	1830.2	6852.21	131.77619	354.98345	0.3712178

Table 4-2 Treatment of Data Obtained with Internal Standard

Sample	Avg Ratio	Corr Ratio	Std Dev		Avg Ar 2/t(m) 2	
A	0.510219		0.014876		(Blank A)	
B	0.488723		0.007606		335.959	
C	0.433996		0.028277			
D	0.412492		0.012147			
A 2	0.587699		0.084273			
E	0.420511	0.365073	0.011577			
F	0.366125	0.317857	0.012554			
Sample	[Ag]/µg/ml	Avg Ratio	Corr Pk Ar	Std Dev		
A & A2	0	0.510219	171.413	4.99790		
B	10	0.488723	164.191	2.55546		
C	20	0.433996	145.805	9.49978		
D	30	0.412492	138.581	4.08084		
E	40	0.365073	122.650	3.88944		
F	50	0.317857	106.787	4.21747		

Table 4-3 Treatment of Data Obtained with Internal Standard

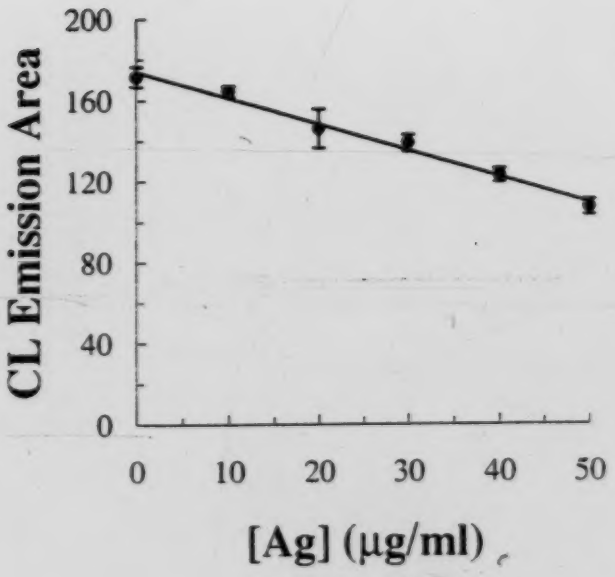

Figure 4-5 Ab*-Ag Calibration Curve with Internal Standard

two graphs were fairly close, indicating a similar rate of decrease of free Ab* both in the presence and absence of microperoxidase.

4.3.4 Extended Calibration Curve

In order to determine the range for which the immunoassay reaction is linear, an extended calibration curve was plotted for 0, 44, 88 and 176 μg/ml of Ag reacting with fixed 53 μg/ml Ab*. No internal standard was used for these experiments. All corrections to peak areas were made as done with the calibration curve without MP. The data is plotted in Figure 4-6. Each data point represents the average peak area of 5 injections and the error bars indicate the standard deviation. From this graph we see that the curve is linear at least up to 88 μg/ml Ag after which it begins to plateau.

4.5 Conclusions

We have demonstrated that chemiluminescence can be used to detect immunoreaction products separated on-chip by capillary electrophoresis, using mouse IgG whole molecule directed against $F(ab')_2$ fragment goat anti-mouse IgG*, HRP conjugate. Unfortunately, we were able to detect only the free Ab* and not the Ab*-Ag complex.

Adsorption may have partly been responsible for the absence of the Ab*-Ag complex. If so, this problem may be eliminated by coating the channel walls with polymeric agents, use of buffer additives[11, 14] or removal of the heavy F_c chains from the Ag. Cleaving the antigen to remove the heavy chains means additional sample

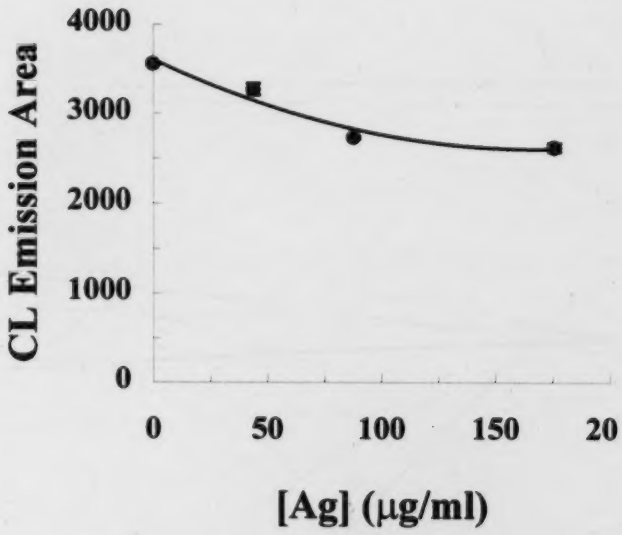

Figure 4-6 Extended Ab*-Ag Calibration Curve

preparation. These added procedures may make the method complex and may be worth doing only if it is cost effective. However, to a greater extent, the problem seemed to be due to precipitation.

The precipitation problem seems to be specific to this immunoassay system and may not occur with other clinically relevant assays. We did some trial runs with HRP-Fl against anti-fluorescein rabbit IgG and did not encounter precipitation problems. However, we were also unable to detect a complex. In this case, co-migration of the complex with the antigen seemed to be the key factor, as shown by a summer student in our group, Kimberly Roy. Using UV absorbance detection on a conventional CE instrument, she was unable to detect a decrease in antigen with increasing antibody. Instead, she saw a broad zone in the region where the antigen peak was expected. We were able to observe a decrease for the HRP-Fl, but no complex peak using chemiluminescence detection on-chip and LIF detection with a conventional CE instrument. This was probably due to quenching of the chemiluminescence and fluorescence of the complex.

Current research in our group was successful in performing similar types of immunoassay reactions using LIF detection.[11] Translation of the LIF conditions used, to our chemiluminescence system may prove to be quite useful. If it is successful, it will take us one step closer to our goal of making the detection system simple by eliminating the need for a source light.

These above modifications require extra work while it may be just sufficient to quantify the reaction by detecting only the free Ab*, as we did. However, our work served to prove that chemiluminescence detection can be applied to microchip capillary electrophoresis separation of immunoassay products.

4.5 References

(1) Campana, A. M. G.; Baeyens, W. R. G.; Zhao, Y. N. *Anal. Chem.* **1997,** *69*, A83-A88.

(2) Rongen, H. A. H.; Hoetelmans, R. M. W.; Bult, A.; Van Bennekom, W. P. *J. Pharm. Biomed. Anal.* **1994,** *12*, 433-462.

(3) Baeyens, W. R. G.; Ling, B. L.; Imai, K.; Calokerinos, A. C.; Schulman, S. G. *J. Microcolumn Sep.* **1994,** *6*, 195-206.

(4) Dadoo, R.; Colon, L. A.; Zare, R. N. *J. High Resolut. Chromatogr.* **1992,** *15*, 133-135.

(5) Weeks, I.; Woodhead, J. S. *Trends in Anal. Chem.* **1988,** *7*, 55-58.

(6) Schultz, N. M.; Tao, L.; Rose, D. J.; Kennedy, R. T. In *Handbook of Capillary Electrophoresis*; Landers, J. P., Ed.; CRC Press, 1996, pp 611-637.

(7) Neupert, W.; Oelkers, R.; Brune, K.; Geisslinger, G. *Prostaglandins* **1996,** *52*, 385-401.

(8) Ekins, R.; Chu, F.; Micallef, J. *J. Biolumin. Chemilumin.* **1989,** *4*, 59-78.

(9) Kricka, L. J.; Carter, T. J. N. In *Clinical and Biochemical Luminescence*; Kricka, L. J., Carter, T. J. N., Eds.; Marcel Dekker: N. Y., 1982; Vol. 12.

(10) van Dyke, K.; McCapra, F.; Behesti, I. *Bioluminescence and Chemiluminescence, Instruments and Applications*; CRC Press: West Palm Beach, Fl, 1985.

(11) Harrison, D. J.; Chiem, N. *Anal. Chem.* **1997, *69***, 373-378.

(12) Towns, J. K.; Regnier, F. E. *Anal. Chem.* **1991,** *63*, 1126.

(13) Lambert, W. J.; Middleton, D. L. *Anal. Chem.* **1990,** *62*, 1585-1587.

(14) Dougherty, A. M.; Cooke, N.; Shieh, P. In *Handbook of Capillary Electrophoresis*; Landers, J. P., Ed.; CRC Press, 1997.

CHAPTER 5

CONCLUSIONS

5.1 Summary

Chemiluminescence detection for microchip capillary electrophoresis has been successfully demonstrated. Optimization of the horseradish peroxidase catalyzed reaction of luminol and hydrogen peroxide was done on-chip and a detection limit of 9 nM for horseradish peroxidase fluorescein conjugated was achieved. The detection system was applied to the immunoassay reaction of $F(ab')_2$ fragment goat anti-mouse IgG and mouse IgG, whole molecule. We demonstrated that at low antigen concentrations, at fixed antibody concentration, the response was linear. At higher antigen concentrations, the calibration curve reached a plateau, indicating saturation of complex formation.

5.2 Evaluation

Although a 9 nM detection limit is not so exciting given the trade-off in separation efficiency and resolution due to large plug sizes, there is still hope for better results. The possibility of using more efficient chemiluminescent systems and use of enhancers for the chemiluminescent reaction seem to provide some room for improvement. [1-4] If these two factors show significant improvement in signal, the need for a large plug size may be eliminated, leading to better separation efficiency and resolution. Alternatively, capillary isotachophoresis (CITP)[5] may be employed for sample stacking in a large plug to produce sharp, narrow bands. This will lead to higher separation efficiency and better resolution. In addition, the double-T injector in the

device may be modified to accommodate larger plug sizes, eliminating the need for single-T injections, so that better reproducibility may be obtained.

Even though we were unable to detect a complex for the immunoassay reaction studied, the possibility exists that the detection scheme may be successful with other systems. The probable precipitation of the complex may have been specific to this particular antibody-antigen system and is certainly not characteristic of all immunoassay systems. As previously demonstrated, microchip CE was quite successful at determining the products of an immunoassay reaction using LIF detection.[6] No problems with precipitation were experienced.

5.3 Applications

Apart from immunoassays, this detection scheme may be employed for the detection of other analytes. The luminol-hydrogen peroxide reaction is catalyzed by Fe (III) complexes, Co (II), Cu (II), Cr (III), Ni (II), Mn (II) and Ti (III) ions, therefore it may be used for the detection of these species.[1, 7, 8] It can also be used for the detection of proteins and amino acids labeled with either HRP (or any of the other protein catalysts described in Chapter 1) or luminol (or any of its derivatives).

The reaction may also be used for the detection of hydrogen peroxide either directly or by coupling to hydrogen peroxide producing reactions.[9] Since hydrogen peroxide is produced by oxidase action of several species, analytes such as glucose, cholesterol, uric acid, sucrose and glucoside metabolites may be quantitated.[1] Therefore, this method can be quite useful for clinical, biochemical and environmental applications.

Trace metal determination is useful for foods, vitamins, pharmaceutical preparations, industrial alloys and water matrices. Protein and amino acid quantitation is of importance to biochemists, and immunoassays are useful for clinical and environmental applications. Chemiluminescence provides a simple, portable and inexpensive means of doing these analyses. This method may also prove to be useful in certain industries for process control, where detection limit is not an issue, but the assurance that a certain level of a particular analyte is present in the correct proportion. For example, it can be used for the determination of the iron content in an iron supplement produced in the pharmaceutical industry.

Currently the detection scheme is still in its early stages and requires further development before it can be put to everyday use in the real world. However, at this point, it may be used for quick, crude, on-site determinations which do not demand a lot in terms of separation efficiency and detection limit.

5.4 Future Directions

Since this detection scheme is still somewhat crude, it requires further development in order to obtain better results. More specifically, detection limit, separation efficiency and resolution should be addressed. The possibility of using enhancers, bigger capillary channels and a larger double-T injector may be exploited in order to improve detection limits. In addition, use of more efficient chemiluminescent systems may be explored. More specifically, the benzoperlene derivative of luminol may be tried as its quantum yield compared to luminol is 700-800 %.[10] Capillary isotachophoresis may be employed to improve separation efficiencies and resolution. In the long term, several other chemiluminescent reactions could be investigated to

determine their suitability for microchip CE. This should open up a whole new world of possibilities for chemiluminescence detection in microchip capillary electrophoresis.

5.5 References

(1) Nieman, T. A. In *Encyclopedia of Analytical Science*; Townshend, A., Ed.; Academic Press, 1995; Vol. 1, pp 608-621.

(2) Sanchez, F. G.; Diaz, A. N.; Garcia, J. A. G. *Journal Of Luminescence* **1995,** *65*, 33-39.

(3) Sun, W.; Ji, X.; Kricka, L. J.; Dunford, H. B. *Can. J. Chem.* **1994,** *72*, 2159-2162.

(4) Diaz, A. N.; Sanchez, F. G.; Garcia, J. A. G. *Journal Of Photochemistry And Photobiology A Chemistry* **1995,** *87*, 99-103.

(5) Burgi, D. S.; Chien, R.-L. In *Handbook of Capillary Electrophoresis*; Landers, J. P., Ed.; CRC Press, 1997.

(6) Harrison, D. J.; Chiem, N. *Anal. Chem.* **1997, *69***, 373-378.

(7) Bowie, A. R.; Sanders, M. G.; Worsfold, P. J. *J. Biolumin. Chemilumin.* **1996,** *11*, 61-90.

(8) Campana, A. M. G.; Baeyens, W. R. G.; Zhao, Y. N. *Anal. Chem.* **1997,** *69*, A83-A88.

(9) Diaz, A. N.; Sanchez, F. G.; Garcia, J. A. G. *Analytica Chimica Acta* **1996,** *327*, 161-165.

(10) Rongen, H. A. H.; Hoetelmans, R. M. W.; Bult, A.; Van Bennekom, W. P. *J. Pharm. Biomed. Anal.* **1994,** *12*, 433-462.